NASA TECHNICAL NOTE

NASA TN D-7678

NASA TN D-7678

PARACHUTE-DEPLOYMENT-PARAMETER IDENTIFICATION BASED ON AN ANALYTICAL SIMULATION OF VIKING BLDT AV-4

by Theodore A. Talay

Langley Research Center

Hampton, Va. 23665

NATIONAL AERONAUTICS AND SPACE ADMINISTRATION • WASHINGTON, D. C. • AUGUST 1974

1. Report No.	2. Government Accession No.	3. Recipient's Catalog No.
NASA TN D-7678		

4. Title and Subtitle	5. Report Date
PARACHUTE-DEPLOYMENT-PARAMETER IDENTIFICATION BASED ON AN ANALYTICAL SIMULATION OF VIKING BLDT AV-4	August 1974
	6. Performing Organization Code

7. Author(s)	8. Performing Organization Report No.
Theodore A. Talay	L-9457
	10. Work Unit No.
9. Performing Organization Name and Address	177-55-35-02
NASA Langley Research Center Hampton, Va. 23665	11. Contract or Grant No.
	13. Type of Report and Period Covered
12. Sponsoring Agency Name and Address	Technical Note
National Aeronautics and Space Administration Washington, D.C. 20546	14. Sponsoring Agency Code

15. Supplementary Notes

Appendix by Theodore A. Talay and W. Douglas Morris.

16. Abstract

A six-degree-of-freedom analytical simulation of parachute deployment dynamics developed at the Langley Research Center is presented. A comparison study was made using flight results from the Viking Balloon Launched Decelerator Test (BLDT) AV-4. Since there are significant voids in the knowledge of vehicle and decelerator aerodynamics and suspension-system physical properties, a set of deployment-parameter input has been defined which may be used as a basis for future studies of parachute deployment dynamics. The study indicates the analytical model is sufficiently sophisticated to investigate parachute deployment dynamics with reasonable accuracy.

17. Key Words (Suggested by Author(s))	18. Distribution Statement
Parachute dynamics Parachute deployment Parachute modeling Viking decelerator system	Unclassified – Unlimited STAR Category 31

19. Security Classif. (of this report)	20. Security Classif. (of this page)	21. No. of Pages	22. Price*
Unclassified	Unclassified	49 52	$3.25

*For sale by the National Technical Information Service, Springfield, Virginia 22151

PARACHUTE-DEPLOYMENT-PARAMETER IDENTIFICATION BASED ON AN ANALYTICAL SIMULATION OF VIKING BLDT AV-4

By Theodore A. Talay
Langley Research Center

SUMMARY

A six-degree-of-freedom analytical simulation of parachute deployment dynamics developed at the Langley Research Center is presented. Voids in the knowledge of vehicle and decelerator aerodynamics and suspension-system physical properties appear to present the major drawbacks to very accurate simulation results. A comparison study was made using flight results from the Viking Balloon Launched Decelerator Test (BLDT) AV-4. Input parameters unknown or not well defined were iteratively adjusted to force an optimum agreement between simulation and flight results of such quantities as vehicle velocity, dynamic pressure, Mach number, tension, attitude, and attitude-rate histories. On the basis of this study, a set of deployment-parameter input has been defined which may be used as a basis for future work in the field of parachute deployment dynamics. The results from the study indicate the analytical model is sufficiently sophisticated to investigate parachute deployment dynamics with reasonable accuracy.

INTRODUCTION

The objective of the Viking '75 mission is to soft-land two science packages on Mars. In order to ensure that guidance and control-system capabilities are not exceeded during the parachute deceleration phase of the landing mission, limits have been established (ref. 1) for the allowable vehicle attitude and attitude rates. The balloon-launched-decelerator test (BLDT) program was conducted in the Earth atmosphere for the purpose of demonstrating the structural integrity and performance of the Viking decelerator system in a range of flight conditions encompassing those postulated for Mars. These flight tests also provided data on the BLDT vehicle attitude and attitude rates. These data are useful in determining whether the Viking attitude and attitude-rate limits may be exceeded.

Although these full-scale tests have been used to demonstrate dynamic performance, especially during the parachute deployment phase, analytical deployment models are warranted since flight conditions at Mars cannot be duplicated precisely on Earth. It is the purpose of the present paper to explain one analytical technique, a six-degree-of-freedom

model of parachute deployment developed at Langley Research Center. This technique was developed from one designed for stable-inflation parachute studies (ref. 2) and the appendix, prepared by the author and W. Douglas Morris of the Langley Research Center, defines the modifications made to it to simulate the entire parachute unfurling and inflation process.

It will be shown that the model helps define input of vehicle, parachute, and suspension-system properties that, for the Viking decelerator system, have been unknown up to now or have had high degrees of uncertainty. This is accomplished through the use of the model by forcing a good correlation between it and flight-test data from BLDT AV-4.

Possible future work would include using the entire set of BLDT flight tests to define further the system input parameters. Once these inputs were well defined, they would be a basis for predicting parachute deployment dynamics and, hence, vehicle attitude and attitude rates for Viking missions with Mars flight conditions.

SYMBOLS

Values are given in both SI and U.S. Customary Units. The measurements and calculations were made in U.S. Customary Units.

$[A']$ direction cosine matrix

$[A']^T$ transpose of direction cosine matrix

C damping coefficient, newton-seconds (pound-seconds)

C_ℓ vehicle aerodynamic rolling-moment coefficient

$\tilde{C}_\ell$ parachute aerodynamic rolling-moment coefficient

$C_{\ell_p} = \dfrac{\partial C_\ell}{\partial \dfrac{pd}{2V_\infty}}$ for vehicle

$\tilde{C}_{\ell_p} = \dfrac{\partial \tilde{C}_\ell}{\partial \dfrac{\tilde{p}D_o}{2V_\infty}}$ for parachute

$$C_{\ell_q} = \frac{\partial C_\ell}{\partial \frac{qd}{2V_\infty}}$$ for vehicle

$$\tilde{C}_{\ell_q} = \frac{\partial \tilde{C}_\ell}{\partial \frac{\tilde{q}D_o}{2V_\infty}}$$ for parachute

$$C_{\ell_r} = \frac{\partial C_\ell}{\partial \frac{rd}{2V_\infty}}$$ for vehicle

$$\tilde{C}_{\ell_r} = \frac{\partial \tilde{C}_\ell}{\partial \frac{\tilde{r}D_o}{2V_\infty}}$$ for parachute

C_m — vehicle aerodynamic pitching-moment coefficient

$\tilde{C}_m$ parachute aerodynamic pitching-moment coefficient

$$C_{m_p} = \frac{\partial C_m}{\partial \frac{pd}{2V_\infty}}$$ for vehicle

$$\tilde{C}_{m_p} = \frac{\partial \tilde{C}_m}{\partial \frac{\tilde{p}D_o}{2V_\infty}}$$ for parachute

$$C_{m_q} = \frac{\partial C_m}{\partial \frac{qd}{2V_\infty}}$$ for vehicle

$$\tilde{C}_{m_q} = \frac{\partial \tilde{C}_m}{\partial \frac{\tilde{q}D_o}{2V_\infty}}$$ for parachute

C_n vehicle aerodynamic yawing-moment coefficient

$\tilde{C}_n$ parachute aerodynamic yawing-moment coefficient

$$C_{n_p} = \frac{\partial C_n}{\partial \frac{pd}{2V_\infty}}$$ for vehicle

$$\tilde{C}_{n_p} = \frac{\partial \tilde{C}_n}{\partial \frac{\tilde{p}D_o}{2V_\infty}}$$ for parachute

$$C_{n_r} = \frac{\partial C_n}{\partial \frac{rd}{2V_\infty}}$$ for vehicle

$$\tilde{C}_{n_r} = \frac{\partial \tilde{C}_n}{\partial \frac{\tilde{r}D_o}{2V_\infty}}$$ for parachute

C_x vehicle aerodynamic axial-force coefficient

$\tilde{C}_x$ parachute aerodynamic axial-force coefficient

C_y vehicle aerodynamic side-force coefficient

$\tilde{C}_y$ parachute aerodynamic side-force coefficient

$$C_{y_p} = \frac{\partial C_y}{\partial \frac{pd}{2V_\infty}}$$ for vehicle

$$\tilde{C}_{y_p} = \frac{\partial \tilde{C}_y}{\partial \frac{\tilde{p}D_o}{2V_\infty}}$$ for parachute

$C_{y_r} = \dfrac{\partial C_y}{\partial \dfrac{rd}{2V_\infty}}$ for vehicle

$\tilde{C}_{y_r} = \dfrac{\partial \tilde{C}_y}{\partial \dfrac{\tilde{r}D_o}{2V_\infty}}$ for parachute

C_z vehicle aerodynamic normal-force coefficient

$\tilde{C}_z$ parachute aerodynamic normal-force coefficient

$C_{z_p} = \dfrac{\partial C_z}{\partial \dfrac{pd}{2V_\infty}}$ for vehicle

$\tilde{C}_{z_p} = \dfrac{\partial \tilde{C}_z}{\partial \dfrac{\tilde{p}D_o}{2V_\infty}}$ for parachute

$C_{z_q} = \dfrac{\partial C_z}{\partial \dfrac{qd}{2V_\infty}}$ for vehicle

$\tilde{C}_{z_q} = \dfrac{\partial \tilde{C}_z}{\partial \dfrac{\tilde{q}D_o}{2V_\infty}}$ for parachute

D_i damping force in each line, newtons (pounds)

D_o nominal parachute diameter, $\left(4S_o/\pi\right)^{1/2}$, meters (feet)

d diameter of test vehicle, meters (feet)

$\{d\}$ column matrix composed of elements dx_i, dy_i, dz_i, meters (feet)

dx_i, dy_i, dz_i displacement of suspension-system attachment points with respect to initial unstressed position, meters (feet)

dx_o, dy_o, dz_o displacement of the confluence point with respect to initial unstressed position, meters (feet)

$\{F\}$ force matrix, newtons (pounds)

F_x^A, F_y^A, F_z^A vehicle aerodynamic forces, newtons (pounds)

$\tilde{F}_x^A, \tilde{F}_y^A, \tilde{F}_z^A$ parachute aerodynamic forces, newtons (pounds)

F_x^C, F_y^C, F_z^C vehicle suspension-system forces, newtons (pounds)

$\tilde{F}_x^C, \tilde{F}_y^C, \tilde{F}_z^C$ parachute suspension-system forces, newtons (pounds)

Fx_o, Fy_o, Fz_o forces applied at confluence point, newtons (pounds)

G_x, G_y, G_z gravity components along vehicle axes, meters/second^2 (feet/second^2)

$\tilde{G}_x, \tilde{G}_y, \tilde{G}_z$ gravity components along parachute axes, meters/second^2 (feet/second^2)

I_{xx}, I_{yy}, I_{zz} moments of inertia about vehicle axis system, kilogram-meters^2 (slug-feet^2)

$\tilde{I}_{xx}, \tilde{I}_{yy}, \tilde{I}_{zz}$ moments of inertia about parachute axis system, kilogram-meters^2 (slug-feet^2)

I_{xy}, I_{xz}, I_{yz} products of inertia about vehicle axis system, kilogram-meters^2 (slug-feet^2)

i arbitrary suspension-system member

$\hat{i}_1, \hat{j}_1, \hat{k}_1$ unit vector in vehicle axis system

K spring constant per suspension-system member, newtons/meter (pounds/foot)

K_{sec} specific secant modulus per suspension-system member, newtons (pounds)

K'_{sec} specific secant modulus per suspension-system member including effect of plastic strain, newtons (pounds)

$K'_{sec,D}$ additional specific secant modulus of damping effects per suspension-system member, newtons (pounds)

K_{TOT} spring constant including effects of plastic deformation and damping per suspension-system member, newtons/meter (pounds/foot)

$\left[K_{TOT}\right]$ matrix of K_{TOT} of all suspension-system members

K'_{TOT} specific secant modulus including effects of plastic strain and damping per suspension-system member, newtons (pounds)

$\ell_{o,i}$ original unstressed suspension-system member lengths, meters (feet)

$\{\ell_o\}$ matrix of original unstressed suspension-system member lengths, meters (feet)

M mass of vehicle, kilograms (slugs)

$\tilde{M}$ mass of parachute, kilograms (slugs)

$\tilde{M}_x,\tilde{M}_y,\tilde{M}_z$ parachute-system mass components in parachute axis system including that due to enclosed and apparent air mass, kilograms (slugs)

$M_x{}^A,M_y{}^A,M_z{}^A$ vehicle aerodynamic moments, newton-meters (pound-feet)

$\tilde{M}_x{}^A,\tilde{M}_y{}^A,\tilde{M}_z{}^A$ parachute aerodynamic moments, newton-meters (pound-feet)

$M_x{}^C,M_y{}^C,M_z{}^C$ vehicle suspension-system moments, newton-meters (pound-feet)

$\tilde{M}_x{}^C,\tilde{M}_y{}^C,\tilde{M}_z{}^C$ parachute suspension-system moments, newton-meters (pound-feet)

p,q,r vehicle-axis components of vehicle inertial angular velocity, degrees/second

$\tilde{p},\tilde{q},\tilde{r}$ parachute-axis components of parachute inertial angular velocity, degrees/second

q_∞ free-stream dynamic pressure, newtons/meter^2 (pounds/foot^2)

$|\text{Rate}_{max}|$ absolute value of maximum attitude rate, degrees/second

$\vec{R}_1$ inertial position vector of vehicle center of gravity, meters (feet)

$\vec{R}_2$ inertial position vector of parachute center of gravity, meters (feet)

$r_{1x,1}, r_{1y,1} r_{1z,1}$ scalar components of a vector from one bridle-leg attachment point on vehicle to parachute center of gravity in vehicle axis system, meters (feet)

$\vec{r}_1$ vector from one bridle-leg attachment point to parachute center of gravity in vehicle axis system, meters (feet)

S vehicle reference area, $\pi d^2/4$, meters^2 (feet^2)

S_o parachute nominal area, meters^2 (feet^2)

S_p canopy inlet area, meters^2 (feet^2)

T suspension-system tension measured at vehicle, newtons (pounds)

$V_{x,1}, V_{y,1}, V_{z,1}$ X-, Y-, and Z-velocity components of vehicle center of gravity along vehicle axes, meters/second (feet/second)

$\tilde{V}_{x,1}, \tilde{V}_{y,1}, \tilde{V}_{z,1}$ X-, Y-, and Z-velocity components of parachute center of gravity along vehicle axes, meters/second (feet/second)

$\vec{V}_1$ inertial velocity vector of vehicle center of gravity, meters/second (feet/second)

$\vec{V}_2$ inertial velocity vector of parachute center of gravity, meters/second (feet/second)

V_∞ free-stream velocity of center of gravity of vehicle or parachute, meters/second (feet/second)

X,Y,Z rectangular Cartesian axes

$\Delta X_i' = x_{p,i}' - x_{o,0} - dx_o$, meters (feet)

$\Delta Y_i' = y_{p,i}' - y_{o,0} - dy_o$, meters (feet)

$\Delta Z_i' = z_{p,i}' - z_{o,0} - dz_o$, meters (feet)

x,y,z vehicle station coordinates, meters (feet)

$\tilde{x}$ longitudinal distance of parachute aerodynamic reference center from parachute center of gravity, meters (feet)

$\bar{x},\bar{y},\bar{z}$ x-, y-, and z-distances from vehicle aerodynamic reference to vehicle center of gravity, meters (feet)

$\dot{x}_{B_I},\dot{y}_{B_I},\dot{z}_{B_I}$ inertial velocity of vehicle center of gravity along vehicle axes, meters/second (feet/second)

$\dot{\tilde{x}}_{B_I},\dot{\tilde{y}}_{B_I},\dot{\tilde{z}}_{B_I}$ inertial velocity of parachute center of gravity along parachute axes, meters/second (feet/second)

$\dot{\tilde{x}}_{W_I},\dot{\tilde{y}}_{W_I},\dot{\tilde{z}}_{W_I}$ inertial wind velocity at parachute in parachute axis system, meters/second (feet/second)

$\ddot{x}_{B_I},\ddot{y}_{B_I},\ddot{z}_{B_I}$ inertial acceleration of vehicle center of gravity along vehicle axes, meters/second^2 (feet/second^2)

$\ddot{\tilde{x}}_{B_I},\ddot{\tilde{y}}_{B_I},\ddot{\tilde{z}}_{B_I}$ inertial acceleration of parachute center of gravity along parachute axes, meters/second^2 (feet/second^2)

$x_{o,0},y_{o,0},z_{o,0}$ original x-, y-, and z-coordinates of confluence point, meters (feet)

$x_{p,i}',y_{p,i}',z_{p,i}'$ coordinates (with respect to parachute axis system) of attachment point i including effects of plastic deformation, meters (feet)

α angle of attack (see fig. 2), degrees

α_T total angle of attack (see fig. 2), degrees

β angle of sideslip (see fig. 2), degrees

δ_i elastic deformation of suspension-system member, meters (feet)

ϵ elastic strain of suspension-system member, meters/meter (feet/foot)

ξ_i', ψ_i', ϕ_i' angles between suspension-system member i and parachute X-, Y-, and Z-axes, degrees

$\xi_{i_0}, \psi_{i_0}, \phi_{i_0}$ original angles between suspension-system member i in unstressed position and parachute X-, Y-, and Z-axes, degrees

$\rho_i', \tau_i', \sigma_i'$ $\left(\cos \xi_i' - \cos \xi_{i_0}\right), \left(\cos \psi_i' - \cos \psi_{i_0}\right), \left(\cos \phi_i' - \cos \phi_{i_0}\right)$, degrees

$\left\{(\rho')^2 + (\tau')^2 + (\sigma')^2\right\}$ column matrix composed of the elements ρ_i', τ_i', and σ_i'

$\vec{\rho}_1$ vector from vehicle center of gravity to vehicle bridle-leg attachment point, meters (feet)

$\rho_{1x,1}, \rho_{1y,1}, \rho_{1z,1}$ x-, y-, and z-coordinates of vehicle attachment point of bridle leg 1 in vehicle axis system, meters (feet)

$\omega_{x_I}, \omega_{y_I}, \omega_{z_I}$ inertial vehicle angular velocity components about vehicle axes, degrees/second

$\dot{\omega}_{x_I}, \dot{\omega}_{y_I}, \dot{\omega}_{z_I}$ time rate of change of inertial vehicle angular velocity components about vehicle axes, degrees/second^2

$\tilde{\omega}_{x_I}, \tilde{\omega}_{y_I}, \tilde{\omega}_{z_I}$ inertial parachute angular velocity components about parachute axes, degrees/second

$\dot{\tilde{\omega}}_{x_I}, \dot{\tilde{\omega}}_{y_I}, \dot{\tilde{\omega}}_{z_I}$ time rate of change of inertial parachute angular velocity components about parachute axes, degrees/second^2

$\omega_{x,1}, \omega_{y,1}, \omega_{z,1}$ angular velocity components of vehicle about vehicle axes, degrees/second

$\vec{\omega}_1$ angular velocity vector of vehicle, degrees/second

Subscripts:

bl bridle leg

fs	full scale
I	inertial
i	suspension-system member
mf	mortar firing
o	confluence point
p	parachute
si	stable inflation
sl	suspension line
v	vehicle

Notation:

·	first derivative with respect to time
··	second derivative with respect to time
'	includes effects of plastic deformation
~	refers to those concerned with parachute

FLIGHT-TEST DESCRIPTION

The BLDT system (see fig. 1) consisted of the test vehicle and the Viking decelerator system. The test vehicle was externally similar in configuration to a Viking entry vehicle with the exception of rocket motors used to accelerate the test vehicle on powered flights. The decelerator system consisted of a 16.15-m (53-ft) nominal-diameter D_o disk-gap-band parachute with 48 suspension lines $1.7D_o$ in length. Three bridle legs, each 2.29 m (7.5 ft) in length, were attached axisymmetrically to the test vehicle. The suspension lines and bridle legs met at the confluence point where a swivel was located. The parachute, located in the back of the test vehicle, was ejected by a mortar and unfurled in a lines-first type of deployment.

The BLDT AV-4 test was conducted over the White Sands Missile Range on August 13, 1972. The objective of this particular flight was to demonstrate performance and structual integrity at deployment conditions in excess of maximum postulated Mars dynamic pressure and in excess of Mach 2.0. Actual Mach number was 2.1 and dynamic pressure was 498 N/m^2 (10.4 lb/ft^2).

SIMULATION PROGRAM

The analytical technique used in this simulation is a more general version of one originally intended for parachute studies after stable inflation (ref. 2). The new model presented here is used to simulate the entire parachute unfurling and inflation processes and to predict the resulting influence on the motions of the suspended vehicle. Reference 3 describes the model and simulation technique in general and the appendix defines the modifications made to the original model from reference 2.

Briefly, the vehicle and parachute are considered separate point masses constrained by a suspension system. Figure 2 indicates the use of massless springs with damping to simulate the suspension system. The suspension-line attachment points are constrained to move in a plane surface defined by a canopy inlet area. This parameter is input in tabular form and simulates the complex flexible nature of the inflating canopy. The vehicle is considered rigid; thus, the bridle-leg attachment points are fixed with respect to the vehicle center of gravity. The juncture of the bridle legs and suspension lines (confluence point) seeks a position in space to maintain a static equilibrium of forces. The coordinate axis systems are also shown in figure 2. The vehicle and parachute each possess six degrees of freedom, that is, changes may occur in the spatial and angular displacements in each of the three coordinate directions. In total, therefore, for the entire vehicle-parachute system there are twelve degrees of freedom, but it is customary to speak of the modeling technique simply as a six-degree-of-freedom technique.

Input to the simulation consists of masses, moments of inertia, aerodynamic characteristics and initial state vectors of the vehicle and parachute, suspension-system physical properties, and atmospheric data.

INPUT

In the ideal case, an analytical model would perfectly describe all the physical phenomena that occur and when combined with exact input (i.e., event times, aerodynamic coefficients, physical properties, and initial conditions) would precisely simulate the real-world event being modeled. In general, however, this is not possible. Complexity, cost, and voids in the basic knowledge of decelerator material dynamics and aerodynamic interactions force the acceptance of a less-than-perfect simulation model and inputs that are

suspected of possessing probable errors. When an analytical model is constructed in sufficient detail to describe the desired output quantities attention is centered on the inputs. An iterative procedure is followed to obtain a good correlation, that is, compare desired output quantities with corresponding flight data and then revise those suspect inputs until a desired degree of comparison occurs. The inputs so derived may not correspond exactly to those in a perfect analytical model, that is, may not equal exactly the real-world-event inputs. Also, there is no guarantee that the accepted inputs are unique; there may be other consistent sets of input that yield equally good comparisons. Hopefully, the researcher can justify (based on existing knowledge and experience gained through independent comparison simulations) a set as acceptable to the problem at hand.

Times

Times for significant events (ref. 4) used in the simulation were:

Event	Time from mortar firing, sec
Initiation of deployment (mortar firing)	0.000
End of unfurling and start of inflation (bagstrip)	1.233 (ref. 4)
Aeroshell separation	7.650 (ref. 4)
End of simulation	50.000

Mortar firing represents the initiation of parachute deployment and provides the reference time for the initial conditions at the beginning of unfurling. Bagstrip represents the end of the unfurling process when the simulation switches over to the inflation phase of deployment. The time used for bagstrip was derived from flight data. An analytical model exists (ref. 5) from which bagstrip times may be determined if conditions at mortar firing are known. This is of importance when the six-degree-of-freedom model is used in a predictive mode in the absence of flight data. At aeroshell separation, the vehicle physical properties change and the simulation program is reconfigured to reflect this at the aeroshell-separation time. The simulation proceeds to 50 sec to ensure that the transient deployment motions of the parachute and vehicle are adequately covered.

Aerodynamic Coefficients

The aerodynamic coefficients C_{y_r}, C_{y_p}, C_{z_q}, C_{z_p}, C_{ℓ}, C_{ℓ_q}, C_{ℓ_r}, C_{m_p}, and C_{n_p} for the vehicle and the analogous coefficients for the parachute were unknown and assumed equal to zero in the equations for the aerodynamic forces and moments acting on the system (see the appendix).

Vehicle.- Other vehicle aerodynamic coefficients for the BLDT AV-4 simulation were obtained from wind-tunnel measurements by the manufacturer. The vehicle aerody-

namic roll-damping coefficient, not known experimentally, was obtained from iterative analysis. A constant value of $C_{\ell_p} = -0.125$ resulted which gave a close comparison between the simulated and flight-test vehicle roll-rate histories.

Parachute.- The parachute normal-force coefficients and the pitching and yawing moment coefficients as functions of the total angle of attack of the parachute were obtained from wind-tunnel measurements (ref. 6) at subsonic velocities as no test data were available relating supersonic experience. The parachute pitch and yaw damping coefficients were not known experimentally. A constant input value of $\tilde{C}_{m_q} = \tilde{C}_{n_r} = -0.20$ was obtained through iterative analysis, which damped parachute angular attitude rates which, in turn, helped match the vehicle attitude and attitude-rate simulations with flight-test data.

The axial-force-coefficient curve for the full-scale parachute was obtained from reference 7 but adjusted, through iterative analysis, to higher values in the supersonic Mach number range to match the average vehicle-tension-history simulation with flight-test values. Additionally, the curve was adjusted at the highest Mach numbers to match the first peaks in the tension histories. The results are displayed in figure 3 which presents the axial-force coefficients for the full-scale parachute used in this simulation along with the curve originally presented in reference 7. From experimental data presented in reference 8 for partially inflated parachutes it was determined that the parachute axial-force coefficient is, among other factors, a function of the inlet area ratio, $S_p/S_{p,si}$. A good fit to this functional dependency using the available data was obtained for this simulation study using the following relationship:

$$\tilde{C}_X = \tilde{C}_{X,fs}\left(\frac{S_p}{S_{p,si}}\right)^{1.25} \tag{1}$$

The observed values of atmospheric pressure, density, and speed of sound measured just before the AV-4 flight (ref. 4) were used. Flight-test relative-wind initial conditions were input to initiate deployment (at mortar firing). This provided a comparison between simulated and flight-test relative-wind vehicle velocity, dynamic pressure, and Mach number. However, a no-wind condition was assumed, which meant that relative-wind vehicle velocities were assumed equal to the vehicle inertial velocities. The vehicle trajectory equations required flight-test vehicle inertial velocities. The simulation substituted the relative-wind vehicle velocities instead, and initiated discrepancies in the altitude and flight-path angle. The discrepancy in the altitude calculation was updated during the simulation to reflect the observed altitude. This, in turn, ensured that proper values of pressure, density, and speed of sound were used as they were input as functions of altitude. The discrepancy in flight-path angle was not considered and was believed to have

influenced vehicle velocity, dynamic pressure, and Mach number in the latter stages of the simulation. A more detailed simulation would include an observed wind input.

Physical Properties

Test vehicle.- The test vehicle for the BLDT system is described in detail in reference 4. The front of the test vehicle was a blunted 70^{o} half-angle cone with a maximum diameter d of 3.51 m (11.5 ft) and a nominal projected area S of 9.7 m^2 (103.9 ft^2). The vehicle mass, moments and products of inertia, and center-of-gravity location values were obtained from measurements by the manufacturer (ref. 4). The physical properties of the vehicle at the times an instant after mortar firing and after aeroshell separation are presented below:

Vehicle physical property	Just after mortar firing	After aeroshell separation
Mass, kg (slugs)	817.3 (56.0)	655.3 (44.9)
Inertias:		
I_{xx}, kg-m^2 (slug-ft^2) . . .	592 (437)	355 (262)
I_{yy}, kg-m^2 (slug-ft^2) . . .	454 (335)	308 (227)
I_{zz}, kg-m^2 (slug-ft^2) . . .	437 (322)	290 (214)
I_{xy}, kg-m^2 (slug-ft^2) . . .	0.62 (0.46)	0.58 (0.43)
I_{xz}, kg-m^2 (slug-ft^2) . . .	2.34 (1.73)	5.23 (3.86)
I_{yz}, kg-m^2 (slug-ft^2) . . .	0.22 (0.16)	-0.23 (-0.17)
Location of center of gravity:[1]		
x, cm (in.)	91.47 (36.01)	100.71 (39.65)
y, cm (in.)	0.00 (0.0)	0.00 (0.0)
z, cm (in.)	-3.58 (-1.41)	-4.47 (-1.76)

[1]Zero vehicle station located 8.103 cm (3.19 in.) forward of the virtual vehicle nose (ref. 4).

Parachute.- The parachute for the BLDT system is described in detail in reference 4. It was basically a 16.15-m (53.0-ft) nominal diameter disk-gap-band parachute with a nominal area S_o of 205.0 m^2 (2206.2 ft^2). The parachute mass was taken to be 28.46 kg (1.95 slugs) consisting of the canopy mass and one-third of the suspension-line mass. The author of reference 9 suggests adding one-third of the spring mass to the mass at the end of the spring to model satisfactorily the dynamic response of a mass oscillating at the end of assumed massless springs. In the case of the parachute one-third of the suspension-line mass was added to the canopy mass. The center-of-gravity locations and moment-of-inertia values for the parachute were computed in the program as a function of inputs of canopy inlet area and mass of various components of the canopy and as functions of the calculated parachute included and apparent air mass (see ref. 7).

Suspension-line properties were obtained in laboratory tensile tests of heat sterilized Type 52, 220-denier, 880-pound minimum tensile strength dacron cord. The tests were performed at several strain rates ranging from near zero up to 210 percent per second using a single-pull hydraulic ram device. Nonlinear suspension-line elastic and damping properties were reported in reference 10. These values were used in the initial simulation attempts of the BLDT AV-4 flight test, but it was found that the tensiometer time-history output did not compare favorably with flight-test data with respect to both the frequency of the oscillations and the envelope of amplitude variations. The suspension-line properties were modified by constant factors until the best comparison in tension-oscillations frequency and amplitude envelope was obtained. It is believed this modification is necessary to simulate accurately the effects of a repeated oscillatory dynamic-load history, including time-dependent hysteresis and heating of the material as reported in reference 11. These effects would not have been present in the single-pull tensile tests conducted in reference 10. From the parametric simulation analysis the final values of the suspension-line specific secant modulus per member $K_{sec,sl}$ were 1.25 times the single-pull values used in reference 7 and the suspension-line damping coefficients per member C_{sl} were 0.75 times the values used in reference 7. These properties are presented in figures 4 and 5, respectively, as a function of the suspension-line strain.

It should be noted that 6 members are used to simulate the 48 suspension lines on BLDT so that 1 member is equivalent in the simulation to a grouping of 8 suspension lines. The values of $K_{sec,sl}$ therefore are equivalent to an eight-line grouping of actual suspension lines. Also, the values of C_{sl} are based on an eight-line grouping taken together. The values for each BLDT suspension-line specific secant modulus and damping coefficients are one-eighth of the values shown in figures 4 and 5, respectively.

Nonlinear elastic properties for the bridle legs were obtained from the manufacturer and the input curve of bridle-leg specific secant modulus per member $K_{sec,bl}$ plotted against bridle-leg strain is shown in figure 6. Because bridle-leg damping values were unavailable, a viscous damping coefficient per member of $C_{bl} = 0$ was assumed. This is considered a good approximation due to the very large stiffness and the resulting low strain and strain rates for the bridle legs.

Initial Conditions

At mortar firing for the BLDT AV-4 system the initial conditions for the vehicle and decelerator (still in its deployment bag) were equal. The following conditions were obtained from references 4 and 12:

Vehicle and decelerator parameters	Value at mortar firing	Source of data
Relative velocity, m/sec (ft/sec) . . .	683 (2 240)	Ref. 12
Altitude, m (ft)	44 862 (147 186)	Ref. 4
Flight-path angle, deg	11.50	Ref. 12
Mach number	2.08	Ref. 12
Dynamic pressure, N/m^2 (lb/ft^2) . . .	498 (10.4)	Ref. 12
Angle of attack, deg	-4.1	Ref. 4
Angle of sideslip, deg	-3.1	Ref. 4
Total angle of attack, deg	5.2	Ref. 4
Pitch rate, deg/sec	-14	Ref. 12
Yaw rate, deg/sec	4	Ref. 12
Roll rate, deg/sec	-30	Ref. 12

Reference 12 was used for some of the inputs since it provided more detailed relative-wind histories of the parameters used in the simulation.

Miscellaneous Conditions

There are a number of other input quantities which cannot be categorized precisely under any of the above headings and are for this reason grouped under the general heading of miscellaneous conditions.

In order to simulate the unfurling process (from mortar firing to bagstrip), the analytical model required an input concerning the history of the parachute bag and partially inflated canopy drag area $\tilde{C}_X S_O$. This was defined as the vehicle-felt line tension T divided by the free-stream dynamic pressure q_∞ for a massless decelerator system. The input history used, obtained by using data derived from reference 4, is presented in figure 7. Another required input was the history of suspension-line alinement at the confluence point relative to the free-stream velocity vector which was grossly approximated from data in reference 4. The input values are shown in figure 8. The preceding inputs of drag-area and suspension-line-alinement histories during unfurling represented an input force and angle-of-force application at the confluence point. From the subsequent model analysis the vehicle attitude, attitude rates, and trajectory during the unfurling process were output.

At bagstrip, the analytical model initiated simulation of parachute motion for the inflation phase with the exception of parachute angular rates which were reinitialized. It was assumed that the parachute angular rates about the parachute center of gravity were equal to the angular motion of the parachute relative to the vehicle, that is, solid-body rotation. The values of parachute angular rates about its center of gravity were found, from earlier iterative computer simulations, to affect the vehicle angular-rate histories

obtained. Therefore, from iterative simulations, the parachute angular rates were adjusted to aid in matching the simulated and flight-test vehicle angular-rate histories. The values in this simulation were:

Parachute pitch rate at bagstrip = 15.0 deg/sec

Parachute yaw rate at bagstrip = 0.0 deg/sec

Parachute roll rate at bagstrip = -30.0 deg/sec

The history of canopy-inlet-area ratio throughout the inflation process was a critical input parameter. It described the filling sequence and timing as well as breathing motions prior to the achievement of a stable canopy. In the simulation of BLDT AV-4, the actual inlet-area-ratio history experienced during the flight was used. This inlet-area ratio, presented as figure 9, was based on data obtained from onboard movie-camera film, as given in references 4 and 13. The inlet-area ratio was corrected to account for the longitudinal motions of the canopy inlet resulting from elastic and plastic deformation in the suspension lines. A maximum value of plastic deformation equal to 1.8 m (6 ft), based on postflight measurements (ref. 4), was used as a best estimate. This was allowed to build up as a linear function of time from bagstrip until the loading history stabilized to simulate the time-integrated loading effects on the suspension lines.

RESULTS AND DISCUSSION

Due to voids in the knowledge of decelerator and vehicle aerodynamics and physical properties, a number of the parameters in this simulation were unknown or had such significant degrees of probable error that they were subjected to iterative analysis. These included:

(1) The vehicle aerodynamic roll-damping coefficient

(2) The parachute aerodynamic pitch- and yaw-damping coefficients

(3) The parachute axial-force coefficient

(4) Suspension-line elasticity

(5) Suspension-line damping

(6) Parachute angular rates at bagstrip

(7) Suspension-line permanent deformation

The effects of these probable errors are discussed in the following results.

Figures 10 to 20 present key simulation results using the six-degree-of-freedom analytical program. Figures 10, 11, and 12 show, respectively, vehicle free-stream

velocity, dynamic pressure, and Mach number. Symbols indicate flight-test data and uncertainty bands are shown to note tracking and data-reduction inaccuracies. Up to about 20 sec after mortar firing the simulated values of free-stream velocity, dynamic pressure, and Mach number correspond quite well with flight-test data but thereafter there is a notable divergence which is most probably due to the exclusion of winds from the analysis. Observed winds (ref. 4) approached nearly 50 m/sec (160 ft/sec) at the altitude of parachute deployment and remained nearly so for the time interval of 50 sec used in this simulation. The discrepancies in the output become more important as the vehicle decelerates and the wind velocities become significant compared to the vehicle inertial velocities.

Figures 13 and 14 show flight-test data and the simulations obtained for the suspension-system tension (or vehicle-felt force). Figure 13 represents the suspension-system-tension history from mortar firing to 50 sec. After the transient period of major canopy breathing (approximately the first 5 sec) the tension histories appear to correspond quite closely up until about 30 sec after mortar firing after which consistently lower tension occurs for the simulation. This is attributed to the smaller simulated dynamic-pressure values due to the assumed no-wind condition as discussed earlier.

Figure 14 gives the suspension-system-tension histories (felt by the vehicle) over the first 5 sec after mortar firing where the significant transient behavior occurs. The first opening load simulation value of 58 316 N (13 110 lb) agrees closely with the flight-test value of 58 952 N (13 253 lb). The tension-history data had a probable error uncertainty of ±1112 N (±250 lb) for the BLDT AV-4 flight. The very large variations in tension and the maximum observed tension value (72 043 N (16 196 lb)) are not as well simulated. Several major problems contribute to this result. It is known that a partial canopy collapse occurred at about 3.6 sec after mortar firing after a period of relatively stable inflation (see fig. 9). This indicates some sort of flow or wake interaction. A similar interaction may have caused the very large load variation at about 2.25 sec after mortar firing. The parachute axial-force coefficient is a function of a multitude of parameters such as Mach number, Reynolds number, body geometry, attitude, wake, and body turbulence. For this simulation, however, an average axial-force coefficient as a function of Mach number and body geometry was assumed. The detailed effects of unsteady flow interactions associated with a breathing canopy and the wake effects of the large-diameter test vehicle are not well understood and are not modeled in the simulation program. Thus, the axial-force coefficient used appears valid for predicting average loading behavior but is generally not as good in terms of the large transient-loading oscillations.

As discussed in reference 11, heating and multicyclic loading and unloading of the suspension lines caused hysteresis and plastic deformation. The iterated average values of suspension-line elasticity (fig. 4), damping (fig. 5), and an assumed plastic-deformation

history have been used to model these effects. While this may contribute to a realistic simulation of the overall nature of the load history in terms of oscillation frequency and average loads, a detailed comparison points out the limitations of not having more exact experimental data for repeated loadings. For example, up to about 3.7 sec after mortar firing, in a region of relatively high suspension-line strain rates, the simulation-loading history appears overdamped whereas after 3.7 sec in a region of lower strain rates the oscillations appear underdamped. Because of programing difficulties and large experimental error in the damping data at low strain rates (ref. 10), the suspension-line damping coefficient was assumed to be a function of strain only, and not strain rate. Any future simulation in detail would require knowledge of this functional dependency.

Figures 15, 16, and 17, respectively, show flight-test histories of vehicle pitch, yaw, and roll rate and the corresponding simulation histories using the six-degree-of-freedom analytical model. The table below shows some major characteristics of the pitch and yaw histories to indicate the accuracy of the simulations:

Vehicle angular-rate characteristic	Pitch-rate history		Yaw-rate history	
	Flight test	Simulation	Flight test	Simulation
Time to first node, sec	9	9	15	17
Time to second node, sec	23	25	31	34
Time to third node, sec	39	42	46	50
$\lvert Rate_{max} \rvert$ up to first node, deg/sec	111	105	82	82
$\lvert Rate_{max} \rvert$ between first and second nodes, deg/sec	46	58	34	38
$\lvert Rate_{max} \rvert$ between second and third nodes, deg/sec	28	38	26	27
$\lvert Rate_{max} \rvert$ between third and fourth nodes, deg/sec	24	30	--	--

Generally the vehicle yaw-rate history is better simulated than the pitch-rate history. As indicated in the table, the maximum-rate values calculated up to the first nodal point are very close to those observed in flight but the simulated pitch rate damps out more slowly than the flight-test data indicates.

The comparison of flight-test vehicle roll rate and that obtained in the simulation shows good results with a close match between the flight-test and calculated nodal points (see fig. 17). This indicates that the chosen value for the vehicle roll-rate damping coefficient (not known experimentally) in this flight simulation is a realistic approximation to its true value. It should be noted that the roll-rate histories shown are averaged

curves – the high-frequency oscillations have been dropped in the interest of showing more clearly the overall long-term nature of the roll-rate history.

Figures 18, 19, and 20 present the comparison between the flight derived data and simulation values of vehicle α, β, and α_T, respectively. The flight derived data were secured from reference 12. These data were obtained using a trajectory reconstruction program to obtain the vehicle Euler angles. These Euler angles were combined with data on wind velocity and direction to obtain the values given as flight derived data in figures 18, 19, and 20. Generally, the reconstructed values of the Euler angles may be up to 5.5° different from camera-data Euler angles which, themselves, are believed to have a mean deviation of $\pm 2^{\circ}$ to $\pm 4^{\circ}$. This, coupled with the probable errors in wind data used to derive the vehicle α, β, and α_T, leads to some uncertainty in the flight derived data presented.

It is evident that these simulation results do not compare as well as the previously presented parameters. Generally, the variations in maximum magnitudes of the angles calculated are smaller than for the flight derived values and in the steady state appear to assume a regular harmonic oscillatory motion for the angles of attack and sideslip and a complex harmonic oscillatory motion for the total angle of attack. Several explanations may account for the inaccuracies of the simulation. To begin with, the six-degree-of-freedom simulation program appears to give similar general trends and magnitudes in the simulation of the vehicle attitude rates but has difficulty in matching flight-test results point for point. Integration of vehicle attitude rates gives the angular displacements presented. Thus, the errors present in the rate simulation will carry over in the long-term integration to angular displacements of the vehicle.

Inherent to this explanation are the probable errors in the parachute and physical-property inputs. Previous computer analysis has given evidence that the parachute motion will lead and influence the vehicle motion in a low-frequency mode although the vehicle continues to oscillate in attitude at higher natural frequencies commensurate with its moments of inertia. The parachute angular rates at bagstrip are important inputs in determining subsequent parachute motion and, hence, vehicle motion. The values chosen for the inputs are those that appeared to optimize the vehicle attitude-rate comparison in overall nature. Their values, however, appear to depend upon conditions of the vehicle at mortar firing and would vary from test to test. Further work is indicated to define accurately parachute motion during the unfurling process. Also, knowledge of parachute aerodynamics is severely limited by a lack of test data – notably aerodynamic force, moment, and stability coefficients – performed over a wide range of Mach numbers and possible inflation geometries. While available test data were used in the simulation, no values of the parachute pitch- and yaw-damping coefficients were available. A value was obtained by the iterative process to damp out the parachute motion and, hence, the vehicle motion also. Because of the flexible behavior of the suspension system, it is not clear what con-

stitutes the parachute's moments of inertia for pitch- and yaw-computational purposes. In this simulation the entire suspension-line moments of inertia were included in the computation of the total parachute moments of inertia. These voids in parachute knowledge lead to undefined uncertainties in the parachute angular-motion simulation and, hence, in an indirect sense, in the vehicle angular-motion simulation.

CONCLUSIONS

A six-degree-of-freedom analytical model of parachute deployment dynamics was developed at the Langley Research Center. A comparison study was conducted using the results of the Viking Balloon Launched Decelerator Test (BLDT) AV-4, in an effort to define input parameters that, up to now, have been unknown or ill defined. Based on the results of this study, the following conclusions are made:

1. A number of input parameters previously unknown or not well defined, have been estimated through the use of iterative analysis. These inputs are considered valid for use as a starting basis for future work involving dynamic analysis of the deployment of a supersonic disk-gap-band parachute. In particular, the vehicle aerodynamic roll-damping coefficient and suspension-line elasticity are considered to be well defined. The parachute aerodynamic axial-force coefficient, pitch- and yaw-damping coefficients, and the suspension-line-damping and plastic-deformation history determined for this simulation are considered adequate for use in future simulations. The parachute angular rates, suspension-line alinement during unfurling, canopy drag area during unfurling, and the canopy-inlet-area ratio during inflation are estimated or known for this particular simulation. Future work is needed, however, to define these parameters more generally for use in predictive analysis, by using test data from the other BLDT flights.

2. The six-degree-of-freedom analytical model simulates the overall nature of supersonic disk-gap-band-parachute deployment dynamics to a reasonable degree of accuracy.

3. Significant voids in the knowledge of decelerator technology, particularly with regard to parachute aerodynamic characteristics and suspension-system physical properties, appear to be a major obstacle to obtaining very accurate simulations and to the use of the analytical model in a predictive mode.

Langley Research Center,
National Aeronautics and Space Administration,
Hampton, Va., July 5, 1974.

APPENDIX

MODIFICATIONS TO STABLE-INFLATION PARACHUTE ANALYTICAL TECHNIQUE TO SIMULATE ENTIRE INFLATION PROCESS

By Theodore A. Talay and W. Douglas Morris
Langley Research Center

EQUATIONS OF MOTION

The equations of motion for a vehicle-decelerator system can be formulated by combining the six-degree-of-freedom equations of motion for both the vehicle and parachute subject to the constraint of the suspension system.

The three translational equations of motion for the center of gravity of the vehicle from reference 2 are

$$\begin{Bmatrix} \ddot{x}_{B_I} \\ \ddot{y}_{B_I} \\ \ddot{z}_{B_I} \end{Bmatrix} = \frac{1}{M} \begin{Bmatrix} F_x{}^A + F_x{}^C \\ F_y{}^A + F_y{}^C \\ F_z{}^A + F_z{}^C \end{Bmatrix} + \begin{Bmatrix} G_x \\ G_y \\ G_z \end{Bmatrix} - \begin{bmatrix} 0 & -r & q \\ r & 0 & -p \\ -q & p & 0 \end{bmatrix} \begin{Bmatrix} \dot{x}_{B_I} \\ \dot{y}_{B_I} \\ \dot{z}_{B_I} \end{Bmatrix} \tag{A1}$$

The vehicle aerodynamic forces are determined by

$$\left.\begin{aligned} F_x{}^A &= C_X q_\infty S \\ F_y{}^A &= \left[C_y + C_{y_r}\left(\frac{rd}{2V_\infty}\right) + C_{y_p}\left(\frac{pd}{2V_\infty}\right) \right] q_\infty S \\ F_z{}^A &= \left[C_z + C_{z_q}\left(\frac{qd}{2V_\infty}\right) + C_{z_p}\left(\frac{pd}{2V_\infty}\right) \right] q_\infty S \end{aligned}\right\} \tag{A2}$$

APPENDIX

The three rotational equations of motion of the vehicle about the body axis are

$$\begin{Bmatrix} \dot{\omega}_{x_I} \\ \dot{\omega}_{y_I} \\ \dot{\omega}_{z_I} \end{Bmatrix} = \begin{bmatrix} I_{xx} & -I_{xy} & -I_{xz} \\ -I_{yx} & I_{yy} & -I_{yz} \\ -I_{zx} & -I_{zy} & I_{zz} \end{bmatrix}^{-1} \left\{ \begin{bmatrix} M_x{}^A + M_x{}^C \\ M_y{}^A + M_y{}^C \\ M_z{}^A + M_z{}^C \end{bmatrix} - \begin{bmatrix} 0 & -r & q \\ r & 0 & -p \\ -q & p & 0 \end{bmatrix} \begin{bmatrix} I_{xx} & -I_{xy} & -I_{xz} \\ -I_{yx} & I_{yy} & -I_{yz} \\ -I_{zx} & -I_{zy} & I_{zz} \end{bmatrix} \begin{Bmatrix} \omega_{x_I} \\ \omega_{y_I} \\ \omega_{z_I} \end{Bmatrix} \right\} \tag{A3}$$

The vehicle aerodynamic moments about the center of gravity are

$$\left.\begin{aligned} M_x{}^A &= \left[C_\ell + C_{\ell_p}\left(\frac{pd}{2V_\infty}\right) + C_{\ell_q}\left(\frac{qd}{2V_\infty}\right) + C_{\ell_r}\left(\frac{rd}{2V_\infty}\right) \right] q_\infty Sd - \left(\bar{y}F_z{}^A - \bar{z}F_y{}^A \right) \\ M_y{}^A &= \left[C_m + C_{m_q}\left(\frac{qd}{2V_\infty}\right) + C_{m_p}\left(\frac{pd}{2V_\infty}\right) \right] q_\infty Sd - \left(\bar{z}F_x{}^A - \bar{x}F_z{}^A \right) \\ M_z{}^A &= \left[C_n + C_{n_r}\left(\frac{rd}{2V_\infty}\right) + C_{n_p}\left(\frac{pd}{2V_\infty}\right) \right] q_\infty Sd - \left(\bar{x}F_y{}^A - \bar{y}F_x{}^A \right) \end{aligned}\right\} \tag{A4}$$

The translational and rotational equations of motion of the parachute are different from those given in reference 2 since the inflating parachute is nonrigid and has a variable mass – due to changes in enclosed and apparent air mass (see ref. 7). The three translational equations of motion for the center of gravity of the parachute are

$$\begin{Bmatrix} \ddot{\tilde{x}}_{B_I} \\ \ddot{\tilde{y}}_{B_I} \\ \ddot{\tilde{z}}_{B_I} \end{Bmatrix} = \begin{Bmatrix} \frac{1}{\tilde{M}_x} \\ \frac{1}{\tilde{M}_y} \\ \frac{1}{\tilde{M}_z} \end{Bmatrix} \left\{ \begin{bmatrix} \tilde{F}_x{}^A + \tilde{F}_x{}^C \\ \tilde{F}_y{}^A + \tilde{F}_y{}^C \\ \tilde{F}_z{}^A + \tilde{F}_z{}^C \end{bmatrix} - \begin{bmatrix} \dot{\tilde{M}}_x\left(\dot{\tilde{x}}_{B_I} - \dot{\tilde{x}}_{W_I}\right) \\ \dot{\tilde{M}}_y\left(\dot{\tilde{y}}_{B_I} - \dot{\tilde{y}}_{W_I}\right) \\ \dot{\tilde{M}}_z\left(\dot{\tilde{z}}_{B_I} - \dot{\tilde{z}}_{W_I}\right) \end{bmatrix} \right\} + \begin{Bmatrix} \tilde{G}_x \frac{\tilde{M}}{\tilde{M}_x} \\ \tilde{G}_y \frac{\tilde{M}}{\tilde{M}_y} \\ \tilde{G}_z \frac{\tilde{M}}{\tilde{M}_z} \end{Bmatrix} - \begin{bmatrix} 0 & -\tilde{r} & \tilde{q} \\ \tilde{r} & 0 & -\tilde{p} \\ -\tilde{q} & \tilde{p} & 0 \end{bmatrix} \begin{Bmatrix} \dot{\tilde{x}}_{B_I} \\ \dot{\tilde{y}}_{B_I} \\ \dot{\tilde{z}}_{B_I} \end{Bmatrix} \tag{A5}$$

APPENDIX

The parachute aerodynamic forces are

$$\left.\begin{aligned}
\tilde{F}_x{}^A &= \tilde{C}_x q_\infty S_o \\
\tilde{F}_y{}^A &= \left[\tilde{C}_y + \tilde{C}_{y_r}\left(\frac{\tilde{r}D_o}{2V_\infty}\right) + \tilde{C}_{y_p}\left(\frac{\tilde{p}D_o}{2V_\infty}\right)\right] q_\infty S_o \\
\tilde{F}_z{}^A &= \left[\tilde{C}_z + \tilde{C}_{z_q}\left(\frac{\tilde{q}D_o}{2V_\infty}\right) + \tilde{C}_{z_p}\left(\frac{\tilde{p}D_o}{2V_\infty}\right)\right] q_\infty S_o
\end{aligned}\right\} \tag{A6}$$

For the parachute system, the body axes are assumed to lie at the center of gravity of the parachute and the axes of symmetry (assuming an axisymmetric parachute) are the principal axes. In this case the products of inertia are zero. The rotational equations of motion about the body axes are determined by

$$\begin{Bmatrix} \dot{\tilde{\omega}}_{x_I} \\ \dot{\tilde{\omega}}_{y_I} \\ \dot{\tilde{\omega}}_{z_I} \end{Bmatrix} = \begin{bmatrix} \tilde{I}_{xx} & 0 & 0 \\ 0 & \tilde{I}_{yy} & 0 \\ 0 & 0 & \tilde{I}_{zz} \end{bmatrix}^{-1} \left\{ \begin{bmatrix} \tilde{M}_x{}^A + \tilde{M}_x{}^C \\ \tilde{M}_y{}^A + \tilde{M}_y{}^C \\ \tilde{M}_z{}^A + \tilde{M}_z{}^C \end{bmatrix} - \begin{bmatrix} \dot{\tilde{I}}_{xx} & 0 & 0 \\ 0 & \dot{\tilde{I}}_{yy} & 0 \\ 0 & 0 & \dot{\tilde{I}}_{zz} \end{bmatrix} \begin{Bmatrix} \tilde{\omega}_{x_I} \\ \tilde{\omega}_{y_I} \\ \tilde{\omega}_{z_I} \end{Bmatrix} \right.$$

$$\left. - \begin{bmatrix} 0 & -\tilde{r} & \tilde{q} \\ \tilde{r} & 0 & -\tilde{p} \\ -\tilde{q} & \tilde{p} & 0 \end{bmatrix} \begin{bmatrix} \tilde{I}_{xx} & 0 & 0 \\ 0 & \tilde{I}_{yy} & 0 \\ 0 & 0 & \tilde{I}_{zz} \end{bmatrix} \begin{Bmatrix} \tilde{\omega}_{x_I} \\ \tilde{\omega}_{y_I} \\ \tilde{\omega}_{z_I} \end{Bmatrix} \right\} \tag{A7}$$

For an aerodynamic reference center lying along the axis of symmetry of the parachute, the parachute aerodynamic moments about the center of gravity are given by

$$\left.\begin{aligned}
\tilde{M}_x{}^A &= \left[\tilde{C}_\ell + \tilde{C}_{\ell_p}\left(\frac{\tilde{p}D_o}{2V_\infty}\right) + \tilde{C}_{\ell_q}\left(\frac{\tilde{q}D_o}{2V_\infty}\right) + \tilde{C}_{\ell_r}\left(\frac{\tilde{r}D_o}{2V_\infty}\right)\right] q_\infty S_o D_o \\
\tilde{M}_y{}^A &= \left[\tilde{C}_m + \tilde{C}_{m_q}\left(\frac{\tilde{q}D_o}{2V_\infty}\right) + \tilde{C}_{m_p}\left(\frac{\tilde{p}D_o}{2V_\infty}\right)\right] q_\infty S_o D_o + \tilde{x}\tilde{F}_z{}^A \\
\tilde{M}_z{}^A &= \left[\tilde{C}_n + \tilde{C}_{n_r}\left(\frac{\tilde{r}D_o}{2V_\infty}\right) + \tilde{C}_{n_p}\left(\frac{\tilde{p}D_o}{2V_\infty}\right)\right] q_\infty S_o D_o - \tilde{x}\tilde{F}_y{}^A
\end{aligned}\right\} \tag{A8}$$

The parachute-system masses $\left(\tilde{M}_x,\tilde{M}_y,\tilde{M}_z\right)$, mass rates $\left(\dot{\tilde{M}}_x,\dot{\tilde{M}}_y,\dot{\tilde{M}}_z\right)$, moments of inertia $\left(\tilde{I}_{xx},\tilde{I}_{yy},\tilde{I}_{zz}\right)$, and moment-of-inertia rates $\left(\dot{\tilde{I}}_{xx},\dot{\tilde{I}}_{yy},\dot{\tilde{I}}_{zz}\right)$ are all calculated using a cylindrical-hemisphere model of a variable geometry parachute as given in reference 7. It is necessary to determine the suspension-system forces and moments in order to solve the equations of motion.

SUSPENSION-SYSTEM FORCES

Physical Properties

With the aerodynamic forces and moments known, the problem is finding the forces and moments caused by the suspension system. As indicated in reference 2 the axial force P in each member i of the suspension system is given by

$$P_i = K_i \delta_i \tag{A9}$$

where K_i represents the spring constants and δ_i the elastic deformations of each line.

If the deformations calculated contain plastic deformations, then a modified value of K_i may be found to give the same line forces subject to the same elastic deformations or

$$P_i = K_i' \delta_i' \tag{A10}$$

Equating equations (A9) and (A10) and dividing the elongations by original suspension-system-member lengths $\ell_{o,i}$ to obtain strains, the specific secant modulus that includes plastic strain effects is obtained:

$$K'_{sec,i} = \left(\frac{\epsilon_i}{\epsilon'_i}\right) K_{sec,i} \tag{A11}$$

The damping force in each line is given as

$$D_i = C_i \frac{\dot{\delta}_i}{\ell_{o,i}} = C_i \dot{\epsilon}_i \tag{A12}$$

This may be converted into an additional secant modulus by dividing by ϵ'_i or

$$K'_{sec,D,i} = C_i \frac{\dot{\epsilon}_i}{\epsilon'_i} \tag{A13}$$

The final value of specific secant modulus that possesses both an elastic and plastic strain effect plus a damping effect is obtained by adding equations (A11) and (A13) or

$$K'_{TOT,i} = \left(\frac{\epsilon_i}{\epsilon'_i}\right) K_{sec,i} + \left(\frac{\dot{\epsilon}_i}{\epsilon'_i}\right) C_i \tag{A14}$$

This may be expressed in terms of a total modified spring constant

$$K_{TOT,i} = \frac{K'_{TOT,i}}{\ell_{o,i}} \tag{A15}$$

The values of $\ell_{o,i}$ and an assumed plastic strain history are input. The elastic strains ϵ_i are calculated by the model at each time step and are used to call $K_{sec,i}$ and C_i from the tabular input where they are stored as functions of elastic strain.

Attachment Point Distances

Consider a vector $\vec{r}_1$ (from the vehicle to the parachute as shown in sketch a) which results in the following equation:

$$\vec{r}_1 = \vec{R}_2 - \vec{R}_1 - \vec{\rho}_1 \tag{A16}$$

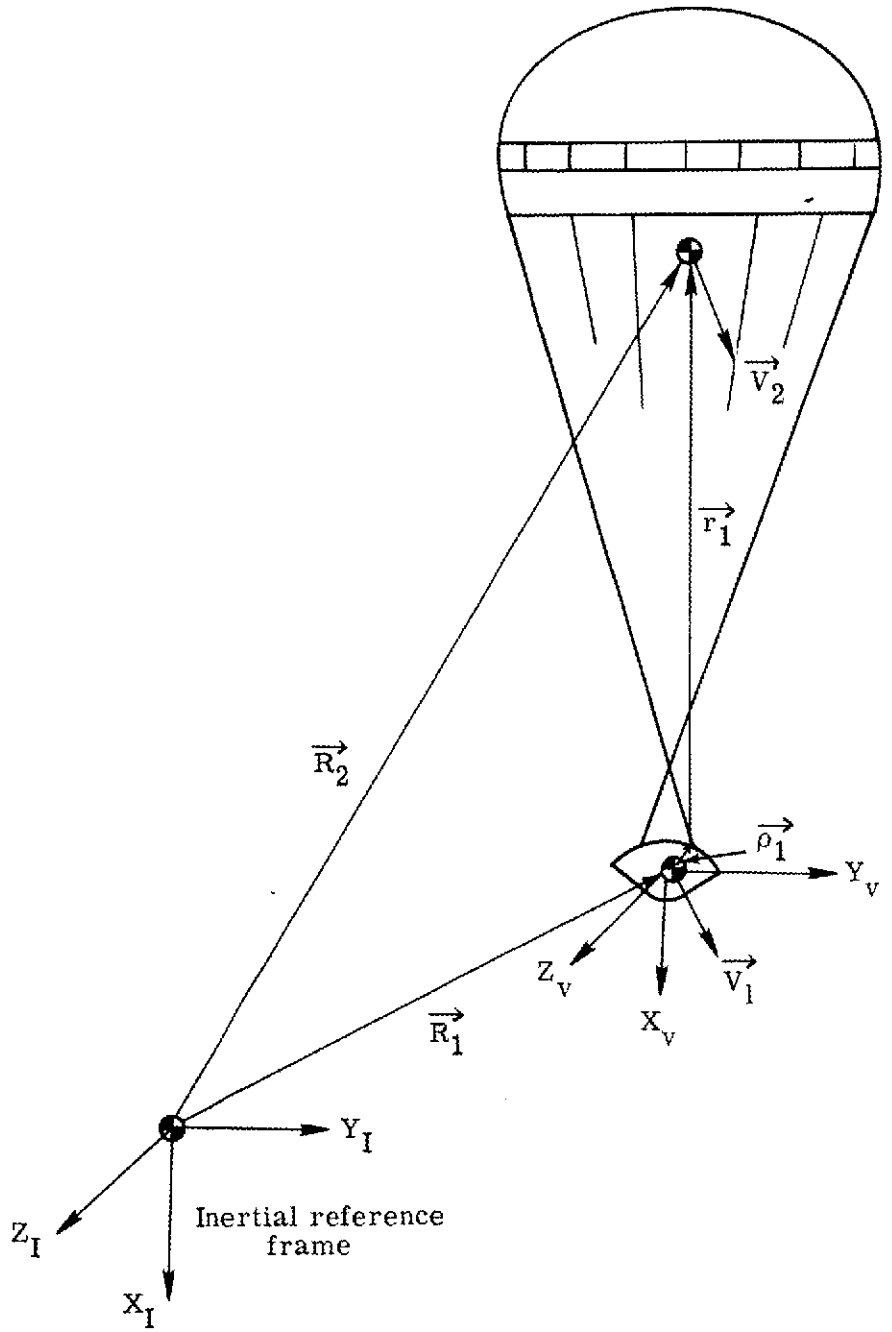

Sketch a.- Vector diagram of model distances.

The time rate of change of $\vec{r}_1$ is given by

$$\dot{\vec{r}}_1 = \dot{\vec{R}}_2 - \dot{\vec{R}}_1 - \dot{\vec{\rho}}_1 \tag{A17}$$

APPENDIX

The vector $\vec{\rho}_1$ is fixed in the vehicle (considered a rigid body) from the center of gravity to one of the bridle-leg attachment points. Taking the derivative of $\vec{\rho}_1$ with respect to time gives

$$\dot{\vec{\rho}}_1 = \vec{\omega}_1 \times \vec{\rho}_1 \tag{A18}$$

The time rates of change of $\vec{R}_1$ and $\vec{R}_2$ are equal to the inertial velocities of the vehicle and the parachute centers of gravity:

$$\left.\begin{aligned} \dot{\vec{R}}_1 &= \vec{V}_1 \\ \dot{\vec{R}}_2 &= \vec{V}_2 \end{aligned}\right\} \tag{A19}$$

The time rate of change of $\vec{r}_1$ in the vehicle reference frame is

$$\dot{\vec{r}}_1 = \dot{r}_{1x,1}\hat{i}_1 + \dot{r}_{1y,1}\hat{j}_1 + \dot{r}_{1z,1}\hat{k}_1 + \vec{\omega}_1 \times \vec{r}_1 \tag{A20}$$

Combining equations (A16) to (A19) yields

$$\dot{r}_{1x,1}\hat{i}_1 + \dot{r}_{1y,1}\hat{j}_1 + \dot{r}_{1z,1}\hat{k}_1 = \vec{V}_2 - \vec{V}_1 - \vec{\omega}_1 \times \vec{\rho}_1 - \vec{\omega}_1 \times \vec{r}_1 \tag{A21}$$

If all vector components are expressed in the vehicle axis system there result three scalar equations for the time rate of change of the components of the vector from the one vehicle bridle-leg attachment point to the parachute center of gravity

$$\left.\begin{aligned} \dot{r}_{1x,1} &= \tilde{V}_{x,1} - V_{x,1} - \omega_{y,1}\left(\rho_{1z,1} + r_{1z,1}\right) + \omega_{z,1}\left(\rho_{1y,1} + r_{1y,1}\right) \\ \dot{r}_{1y,1} &= \tilde{V}_{y,1} - V_{y,1} - \omega_{z,1}\left(\rho_{1x,1} + r_{1x,1}\right) + \omega_{x,1}\left(\rho_{1z,1} + r_{1z,1}\right) \\ \dot{r}_{1z,1} &= \tilde{V}_{z,1} - V_{z,1} - \omega_{x,1}\left(\rho_{1y,1} + r_{1y,1}\right) + \omega_{y,1}\left(\rho_{1x,1} + r_{1x,1}\right) \end{aligned}\right\} \tag{A22}$$

Equations of the same form are obtained for the time rate of change of the components of the vectors from the other bridle-leg attachment points to the parachute center of gravity (expressed in the vehicle axis system). Through transformations, equations (A22) are expressible in the parachute axis system. Integration of these equations will give the instantaneous positions of the bridle-leg attachment points on the vehicle.

APPENDIX

The parachute suspension-line attachment points are also subject to movement with time with respect to the parachute axis system as the parachute inflates or breathes.

The canopy-inlet circle is allowed to expand or contract based upon a history of the inlet-area-ratio input. This determines the y- and z-coordinates of the suspension-line attachment points with respect to the parachute axis system. Also, based upon the parachute model configuration (ref. 7) during inflation and breathing the inlet circle's x-position with respect to the parachute center of gravity is determined.

The total deformed lengths of the suspension-system members, expressed in components with respect to the parachute axis system, are given by

$$\left.\begin{aligned} \Delta X_i' &= x_{p,i}' - x_{o,0} - dx_o \\ \Delta Y_i' &= y_{p,i}' - y_{o,0} - dy_o \\ \Delta Z_i' &= z_{p,i}' - z_{o,0} - dz_o \end{aligned}\right\} \tag{A23}$$

where the prime (') values indicate the effects of plastic deformations. Dividing the member-component lengths by the total member lengths gives the direction cosines with respect to the parachute axis system.

As shown in reference 2 the force components of each suspension-system member with respect to the parachute axis system required to hold the suspension system in equilibrium for a given displacement of the vehicle and parachute can be expressed in terms of the displacements of the points where the forces are applied (coordinates of the suspension-line and bridle-leg attachment points with respect to the original unstressed position) and the original lengths and direction cosines of the suspension-system members. The matrix equation is given as (from ref. 2)

$$\left\{F\right\} = \left[A'\right]\left[K_{TOT}\right]\left[\left[A'\right]^T\left\{d\right\} - \frac{1}{2}\left\{\ell_o\right\}\left\{(\rho')^2 + (\tau')^2 + (\sigma')^2\right\}\right] \tag{A24}$$

where the prime (') indicates the inclusion of plastic deformations and $\left[K_{TOT}\right]$ is the matrix of the total modified spring constants determined by equation (A15).

The confluence point is an interior point in the suspension-system framework and it is assumed that no external forces are applied there. Thus, the forces Fx_o, Fy_o, and Fz_o vanish when the framework is in static equilibrium or

$$\left.\begin{aligned} Fx_o &= 0 \\ Fy_o &= 0 \\ Fz_o &= 0 \end{aligned}\right\} \tag{A25}$$

The results of combining equations (A15) and (A23) to (A25) are three complex nonlinear equations (ref. 2) for the three unknowns dx_o, dy_o, and dz_o – the displacements of the confluence point from its original position. The analysis continues as outlined in reference 2. A Newton-Raphson iterative solution method is employed to converge on the values of dx_o, dy_o, and dz_o. Once the displacements of the confluence point are found, the force components at the attachment points for each suspension-system member are determined by equations (A24). If these force components F_x^C, F_y^C, F_z^C, $\tilde{F}_x^C$, $\tilde{F}_y^C$, and $\tilde{F}_z^C$ are multiplied by the moment arms from the vehicle and parachute centers of gravity, the moment contributions M_x^C, M_y^C, M_z^C, $\tilde{M}_x^C$, $\tilde{M}_y^C$, and $\tilde{M}_z^C$ can be now added to the aerodynamic forces and moments to calculate the six-degree-of-freedom motions of both the vehicle and parachute until the next time step. At the new time step the position equations (A22) are integrated to obtain new displacements of the bridle-leg attachment points and along with the new suspension-line-attachment-point locations obtained from input and parachute-geometry considerations, these are used in the determination of the new confluence point position. From this, new suspension-system forces and moments are computed and so on.

The mathematical model as presented has been programed in FORTRAN IV language for the CDC 6600 computer. The model is run as an integral part of the LRC-MASS program which is a general multiphase trajectory program. The program starts at mortar firing and continues with the unfurling phase until bagstrip when the program changes to the inflation phase. The program is later changed again to reinitialize conditions representing aeroshell separation. The LRC-MASS program is used to compute the translational and rotational motions of the vehicle in three-dimensional space.

REFERENCES

1. Murrow, H. N.; Henke, D. W.; and Eckstrom, C. V.: Development Flight Tests of the Viking Decelerator System. AIAA Paper No. 73-455, May 1973.

2. Gamble, Joe D.: A Mathematical Model for Calculating the Flight Dynamics of a General Parachute-Payload System. NASA TN D-4859, 1968.

3. Talay, Theodore A.; Morris, W. Douglas; and Whitlock, Charles H.: An Advanced Technique for the Prediction of Decelerator System Dynamics. AIAA Paper No. 73-460, May 1973.

4. Dickinson, D.; Schlemmer, J.; Hicks, F.; Michel, F.; and Moog, R. D.: Balloon Launched Decelerator Test Program – Post-Test Test Report (45 Day) – BLDT Vehicle AV-4. TR-3720295 (Contract NAS 1-9000), Martin Marietta Corp., Oct. 20, 1972. (Available as NASA CR-112179.)

5. Poole, Lamont R.; and Huckins, Earle K., III: Evaluation of Massless-Spring Modeling of Suspension-Line Elasticity During the Parachute Unfurling Process. NASA TN D-6671, 1972.

6. Eckstrom, Clinton V.: Development and Testing of the Disk-Gap-Band Parachute Used for Low Dynamic Pressure Applications at Ejection Altitudes at or Above 200,000 Feet. NASA CR-502, 1966.

7. Whitlock, Charles H.; Poole, Lamont R.; and Talay, Theodore A.: Postflight Simulation of Parachute Deployment Dynamics of Viking Qualification Flight Tests. NASA TN D-7415, 1973.

8. Scher, Stanley H.; and Young, Irene G.: Drag Coefficients for Partially Inflated Flat Circular Parachutes. NASA TN D-6423, 1971.

9. Myklestad, N. O.: Vibration Analysis. McGraw-Hill Book Co., Inc., 1944.

10. Poole, Lamont R.: Force-Strain Characteristics of Dacron Parachute Suspension-Line Cord Under Dynamic Loading Conditions. AIAA Paper No. 73-446, May 1973.

11. Moog, R. D.; Bendura, R. J.; Timmons, J. D.; and Lau, R. A.: Qualification Flight Tests of the Viking Decelerator System. AIAA Paper No. 73-457, May 1973.

12. Lundstrom, Reginald R.; Raper, James L.; Bendura, Richard J.; and Shields, E. William: Flight Tests of Viking Parachute System in Three Mach Number Regimes. I – Vehicle Description, Test Operations, and Performance. NASA TN D-7692, 1974.

13. Bendura, Richard J.; Lundstrom, Reginald R.; Renfroe, Philip G.; and LeCroy, Stewart R.: Flight Tests of Viking Parachute System in Three Mach Number Regimes. II – Parachute Test Results. NASA TN D-7734, 1974.

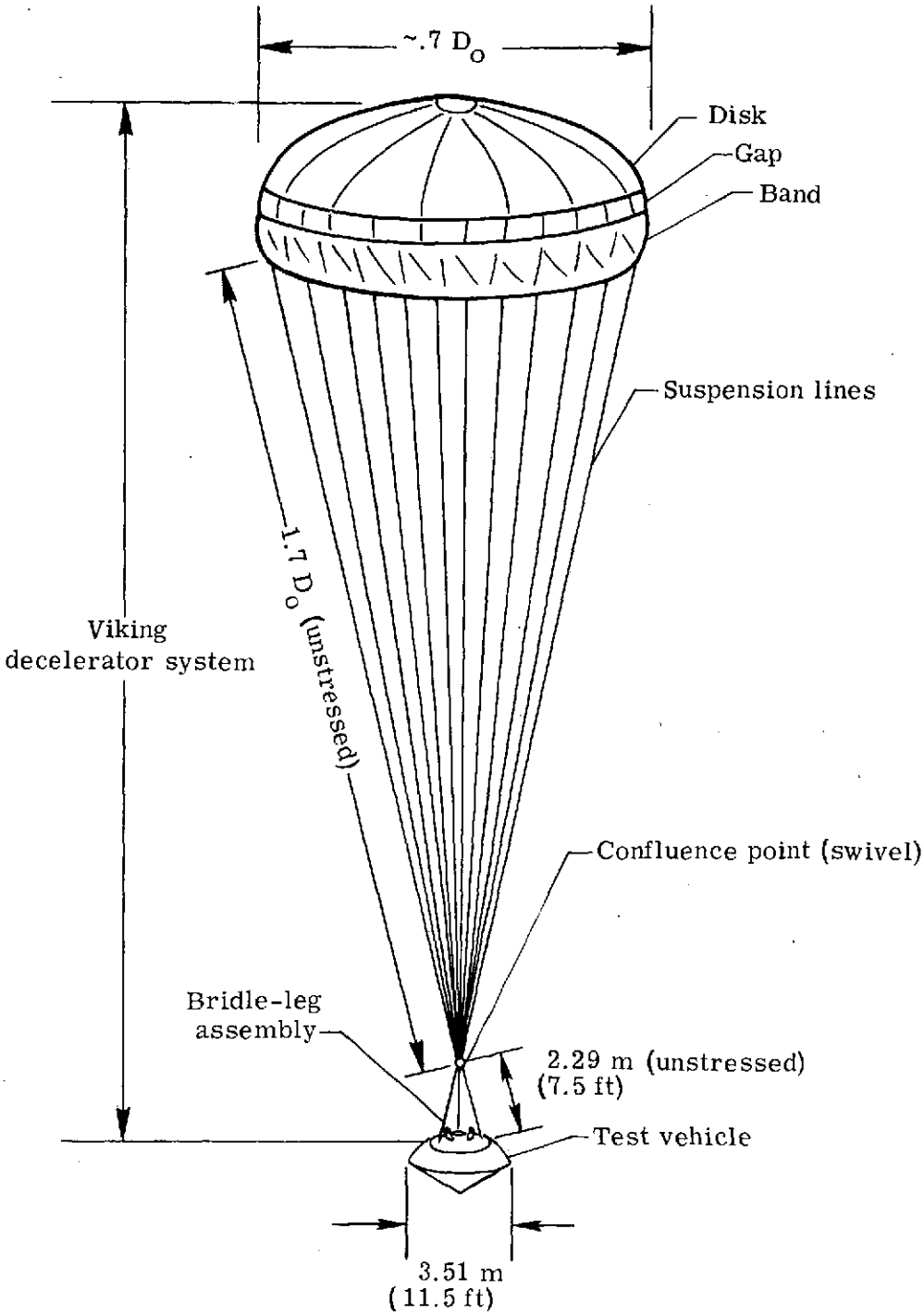

Figure 1.- Balloon-launched-decelerator test (BLDT) system.

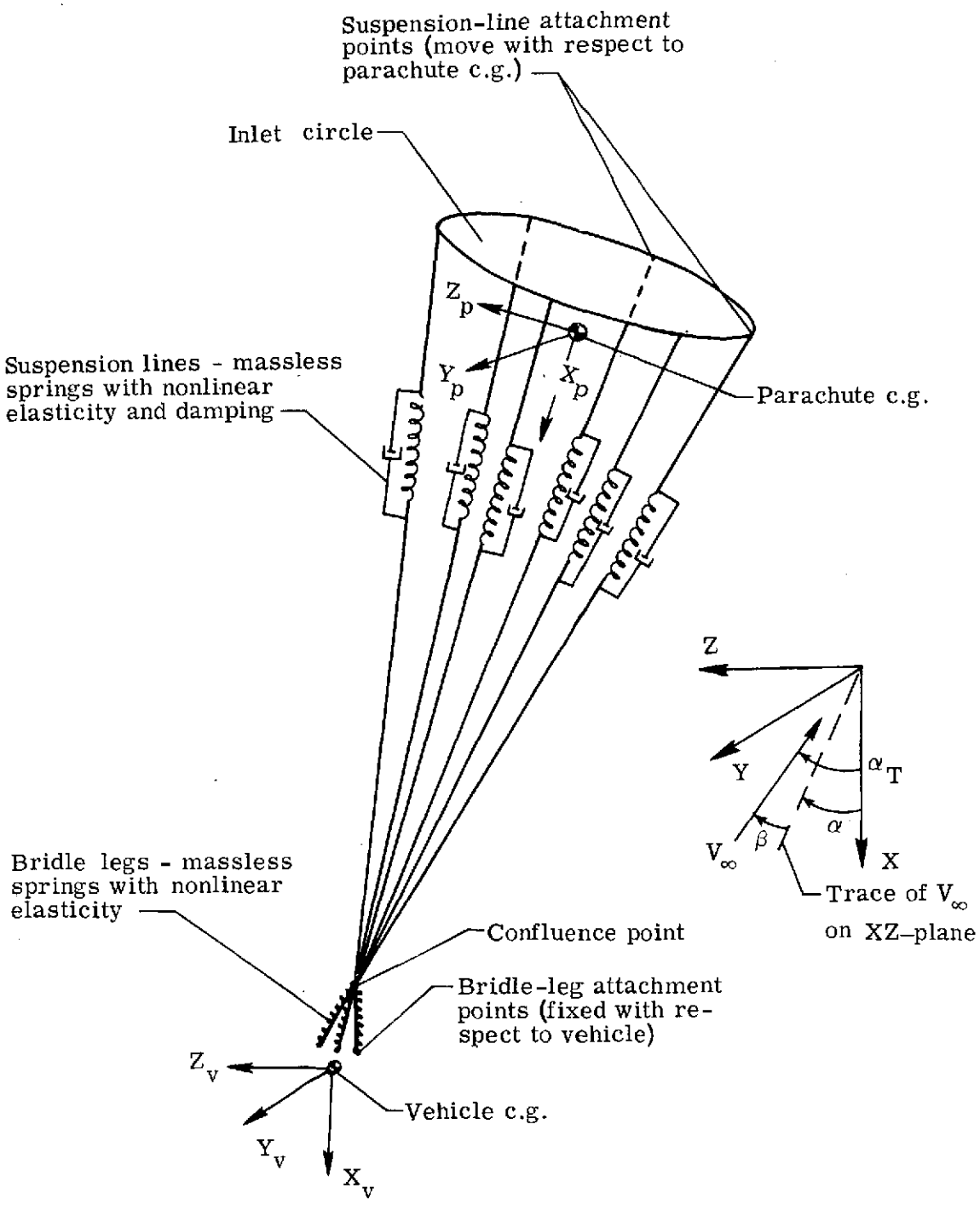

Figure 2.- Six-degree-of-freedom BLDT simulation model.

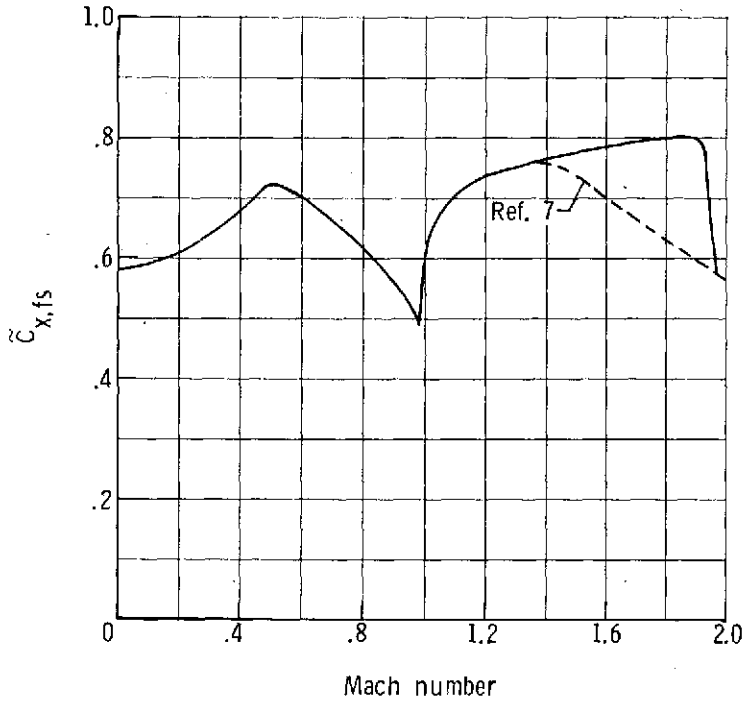

Figure 3.- Parachute axial-force coefficient (full scale).

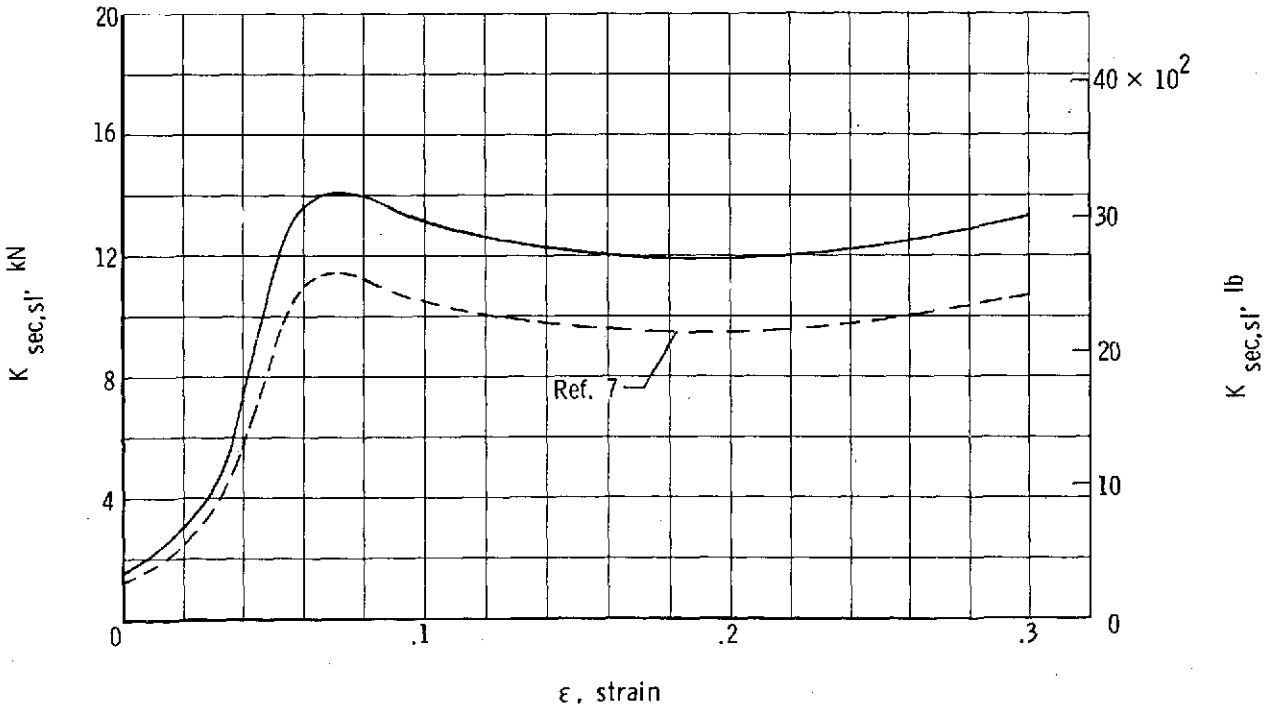

Figure 4.- Suspension-line secant modulus for eight-line grouping.

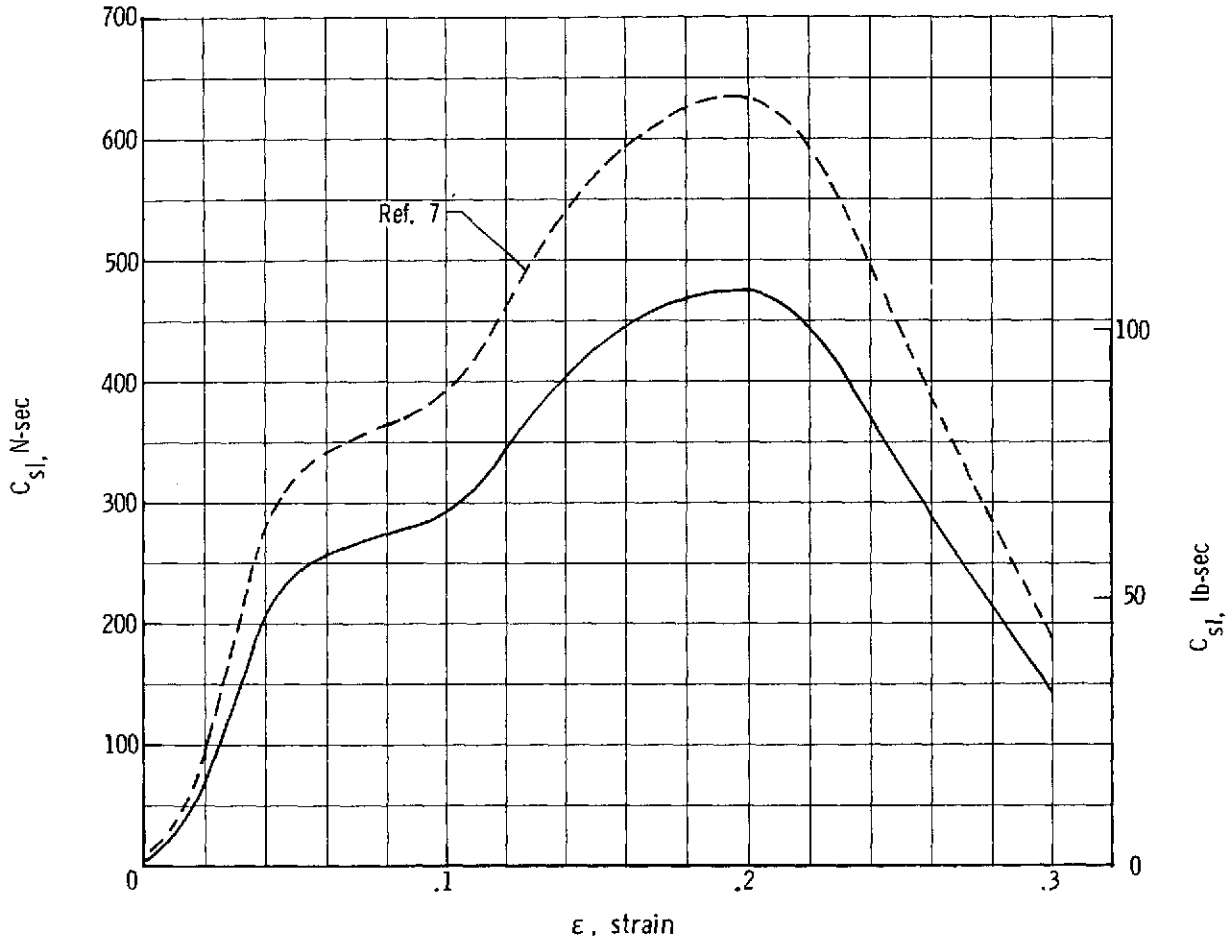

Figure 5.- Suspension-line damping coefficient for eight-line grouping.

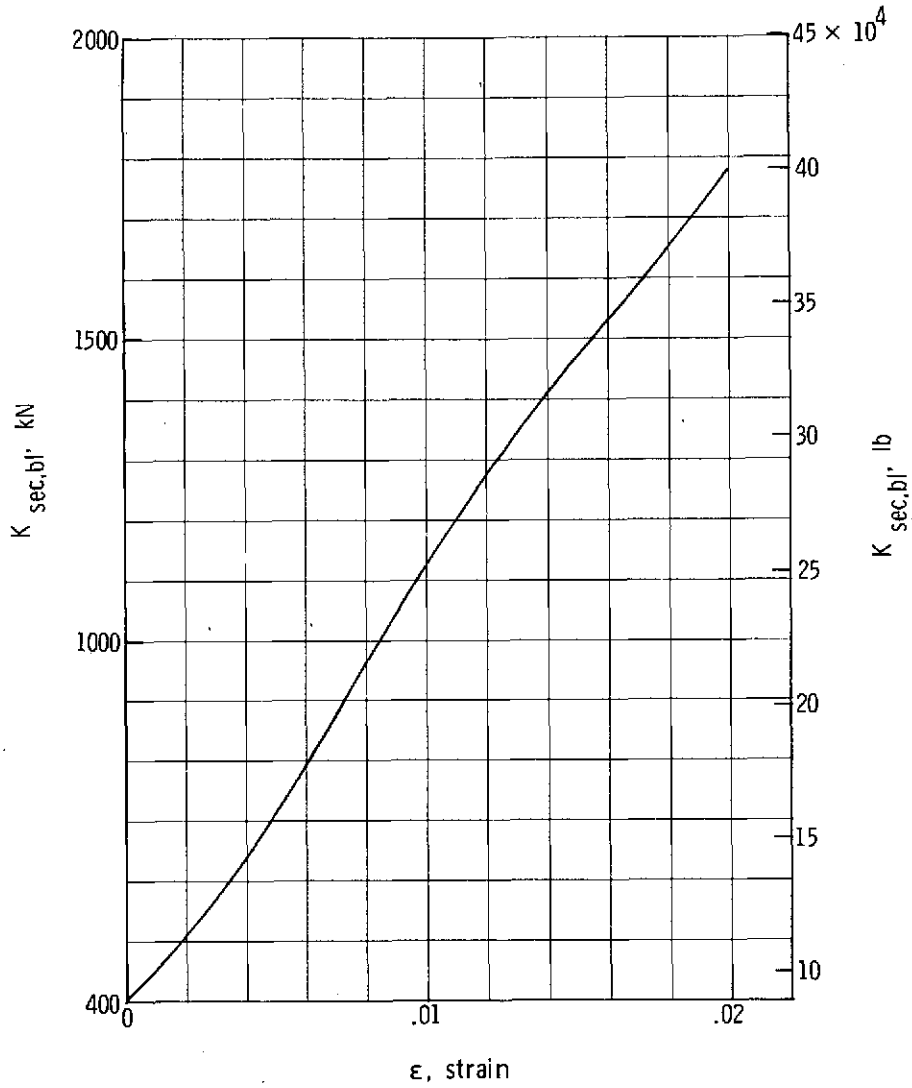

Figure 6.- Bridle-leg secant modulus.

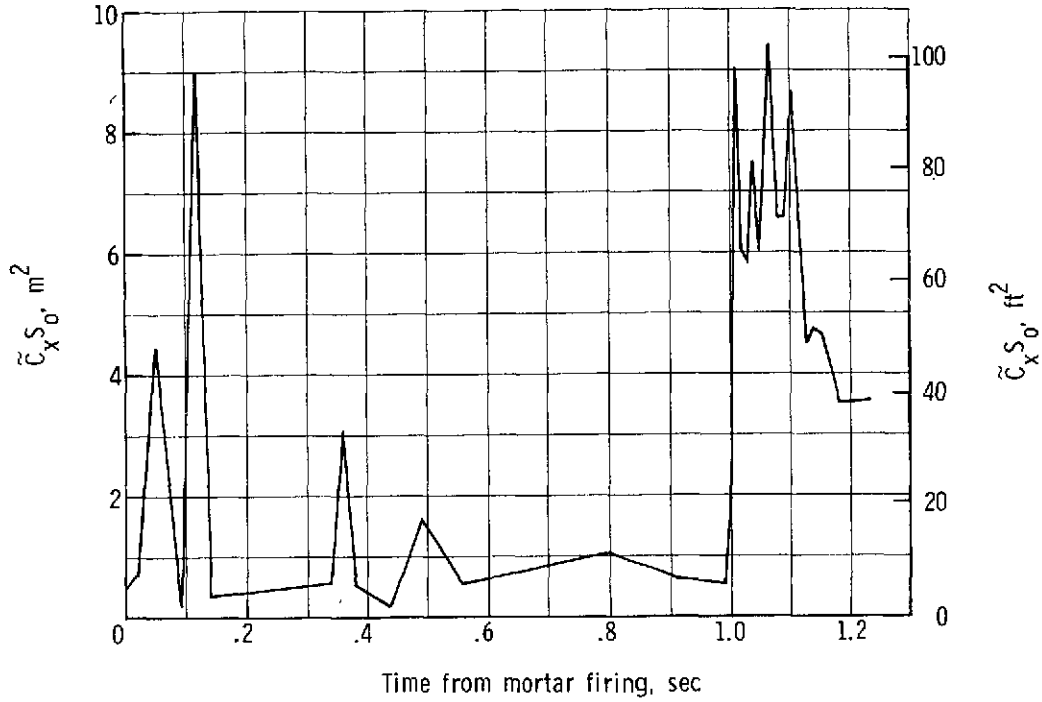

Figure 7.- Axial-force area during parachute unfurling (input to LRC simulation).

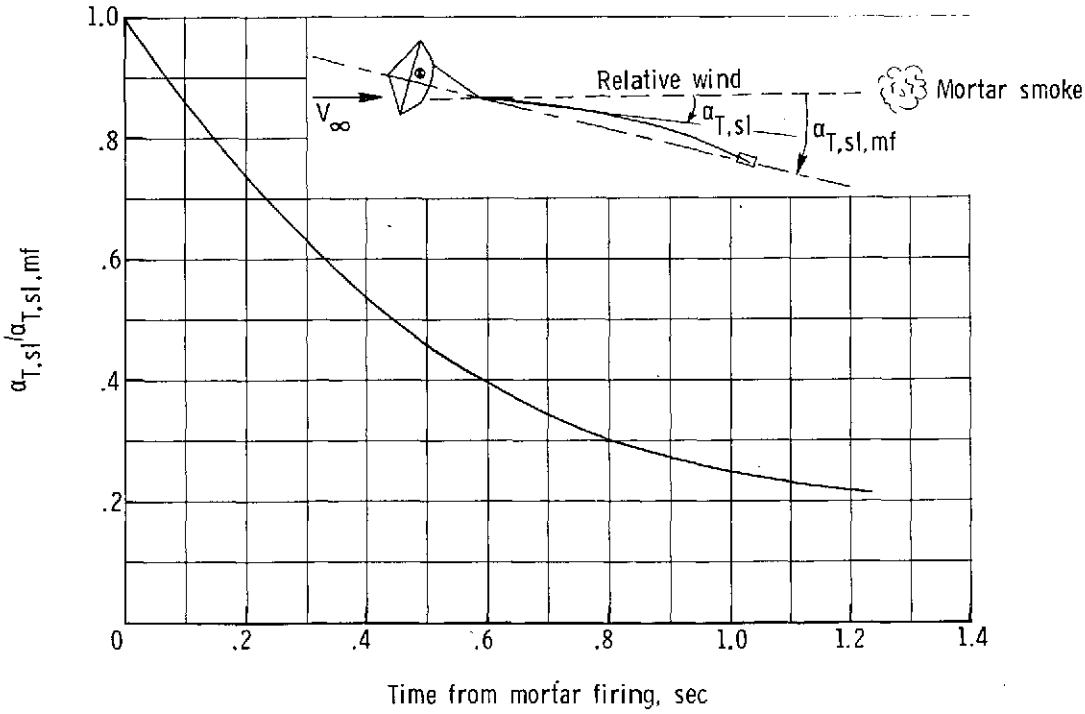

Figure 8.- Suspension-line attitude during parachute unfurling (input to LRC simulation).

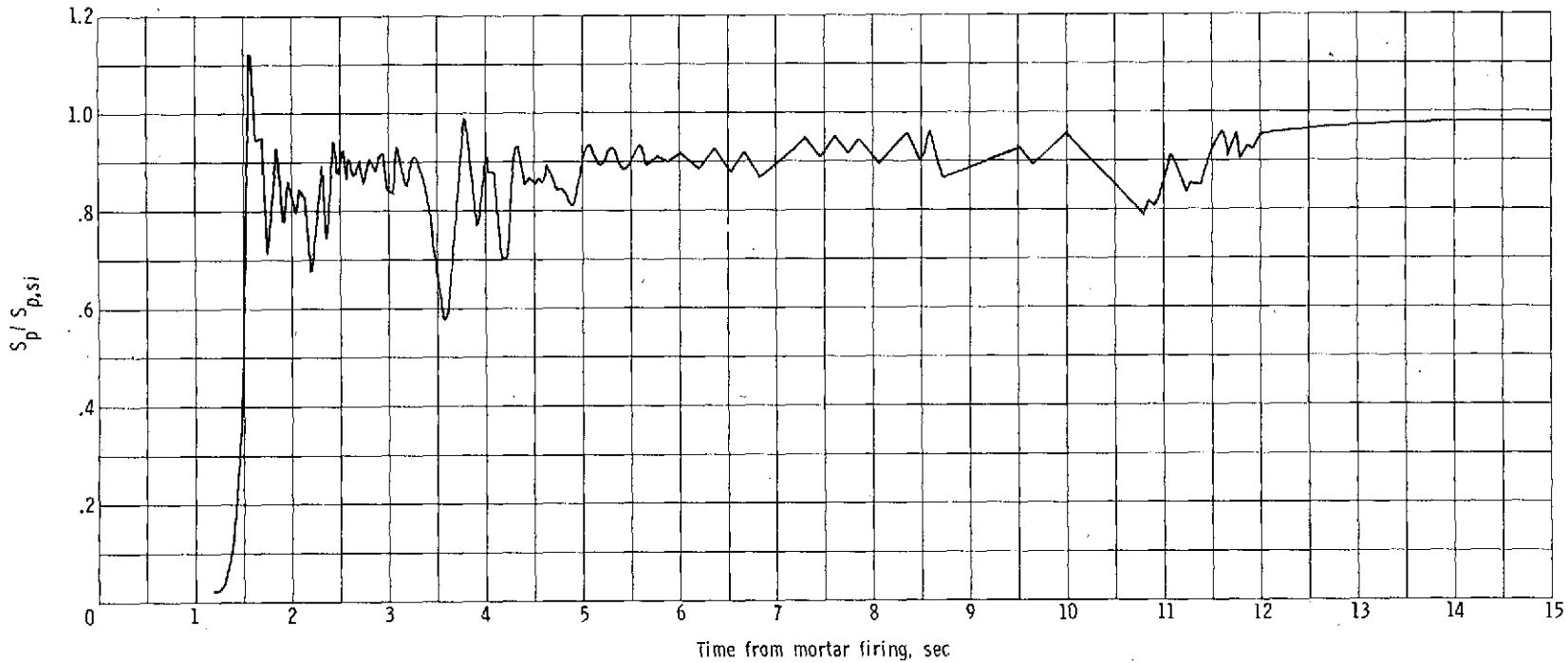

Figure 9.- Canopy-inlet-area ratio.

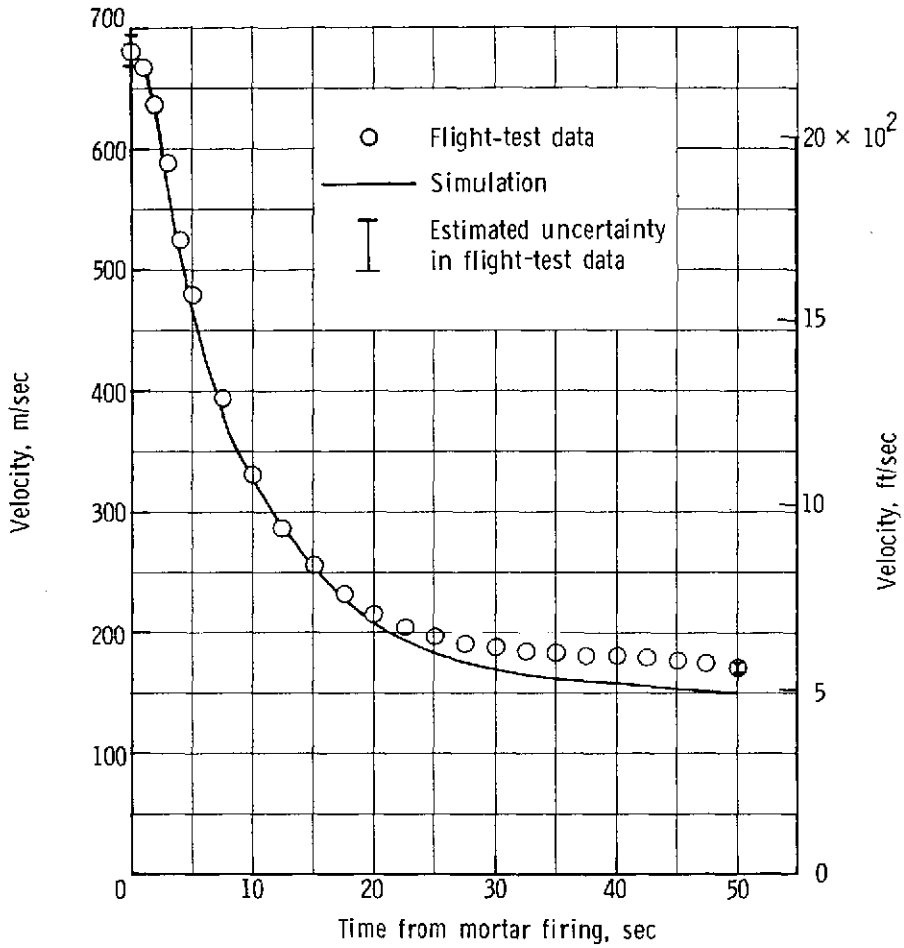

Figure 10.- Free-stream-velocity comparison.

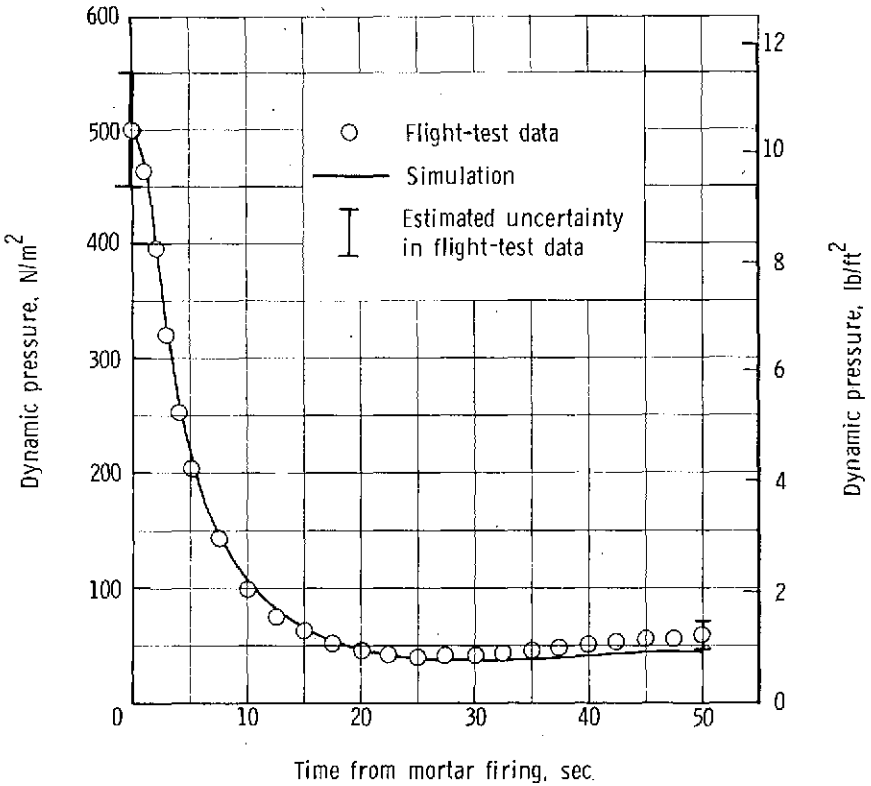

Figure 11.- Free-stream-dynamic-pressure comparison.

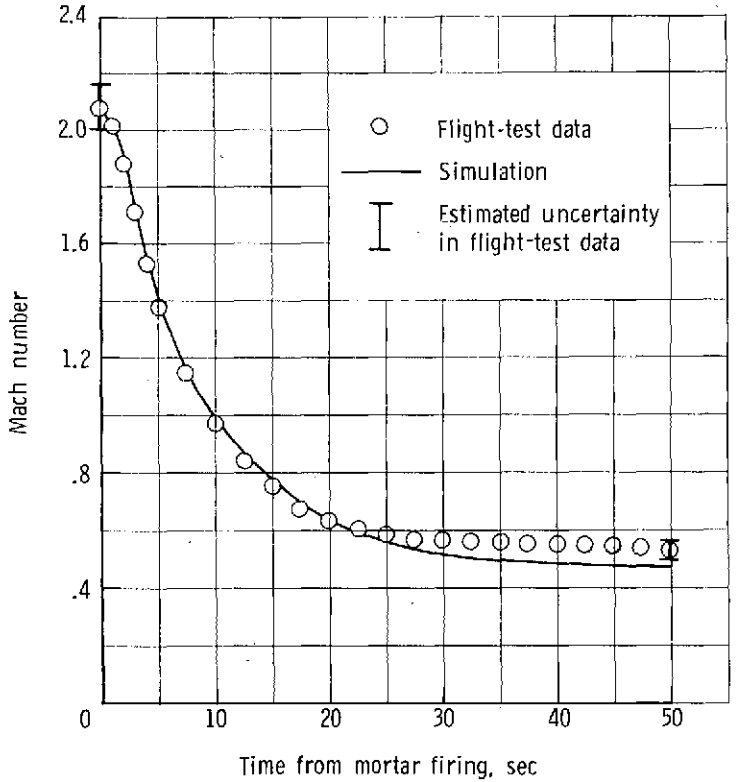

Figure 12.- Free-stream-Mach-number comparison.

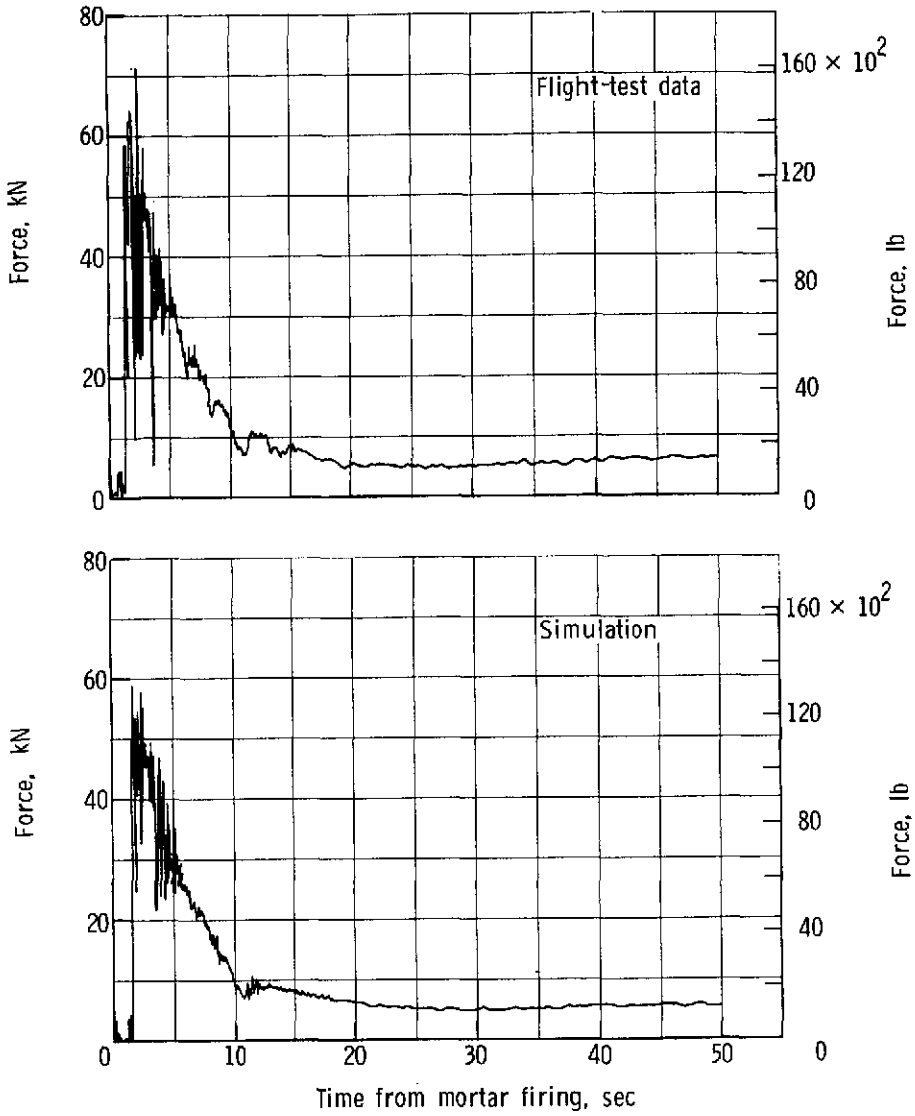

Figure 13.- Suspension-system force comparison from mortar firing to 50 sec.

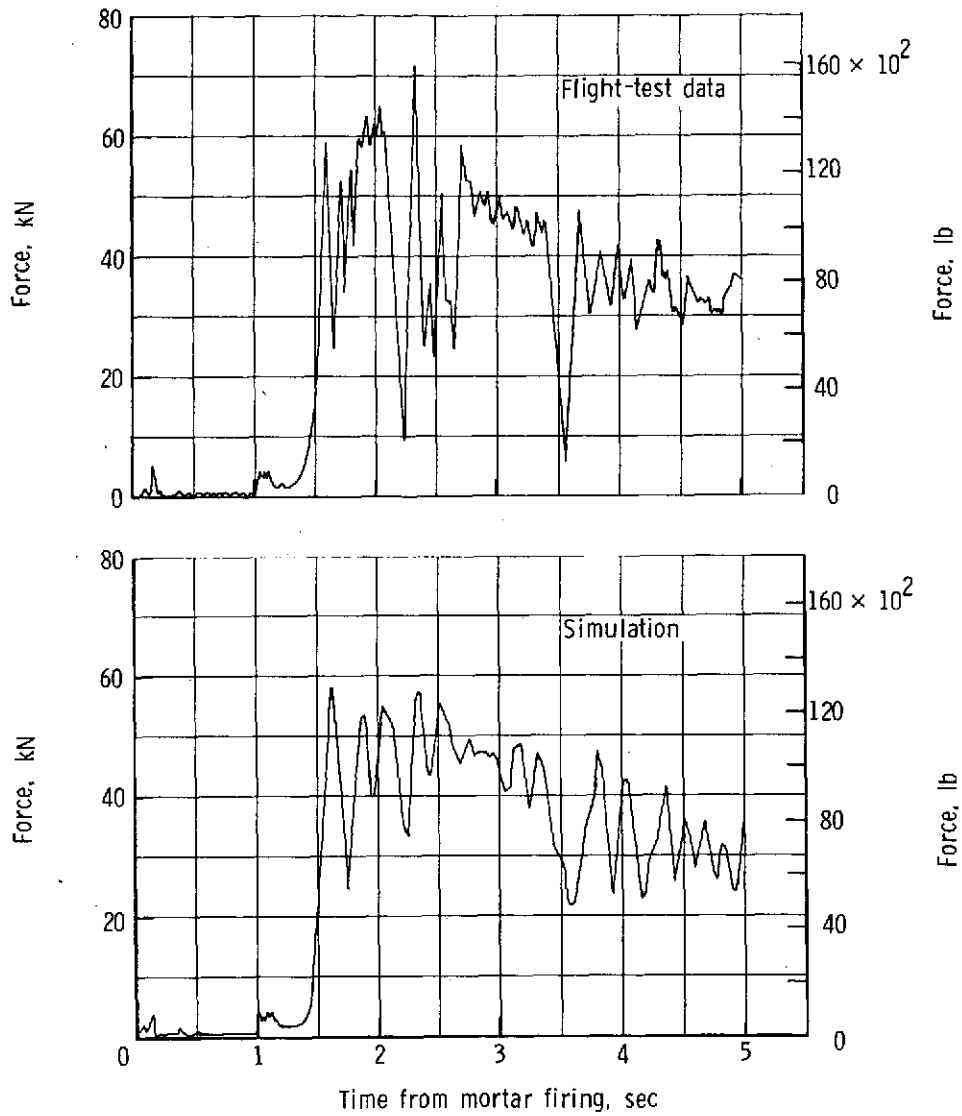

Figure 14.- Suspension-system force comparison from mortar firing to 5 sec.

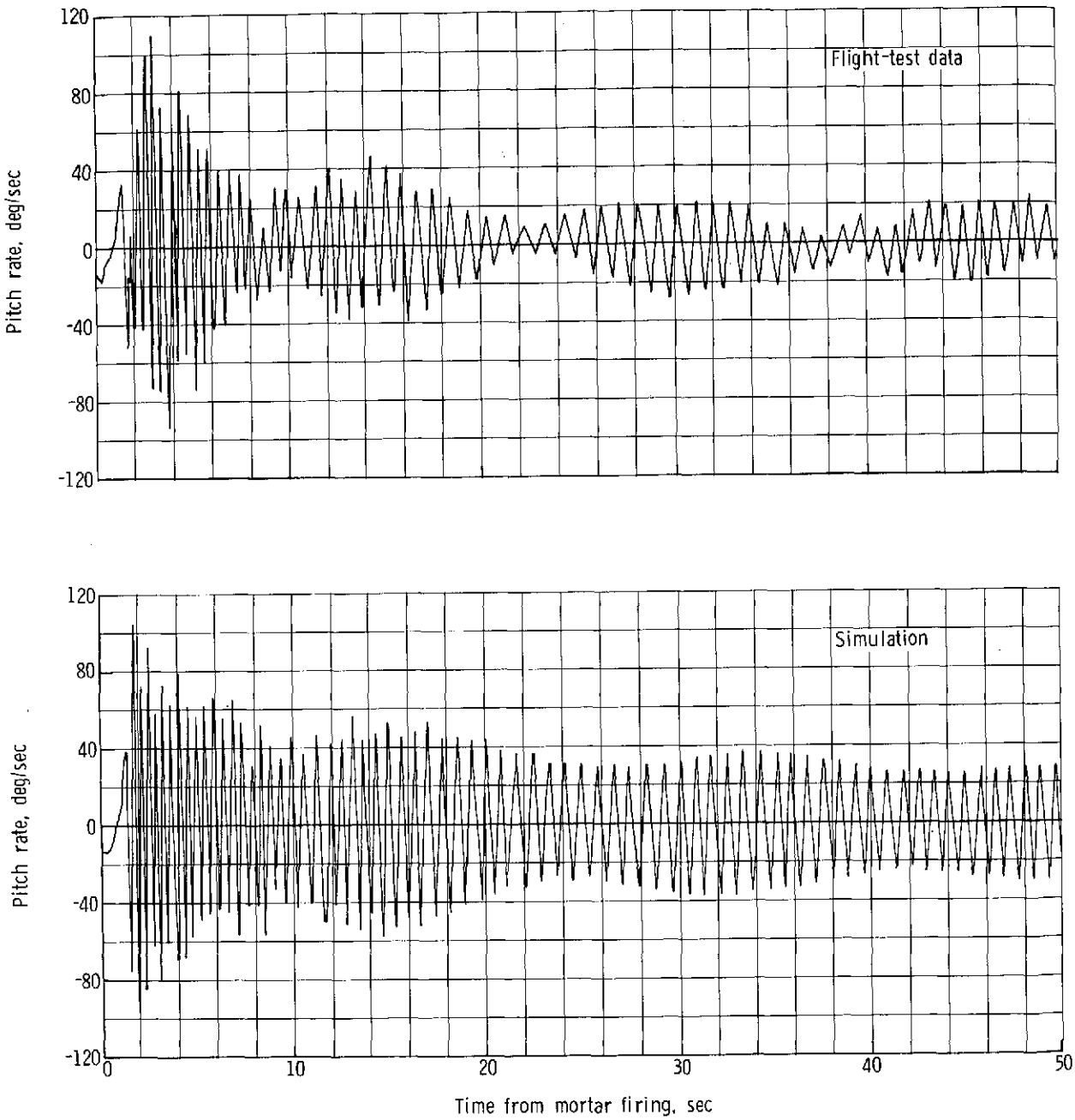

Figure 15.- Vehicle pitch-rate comparison.

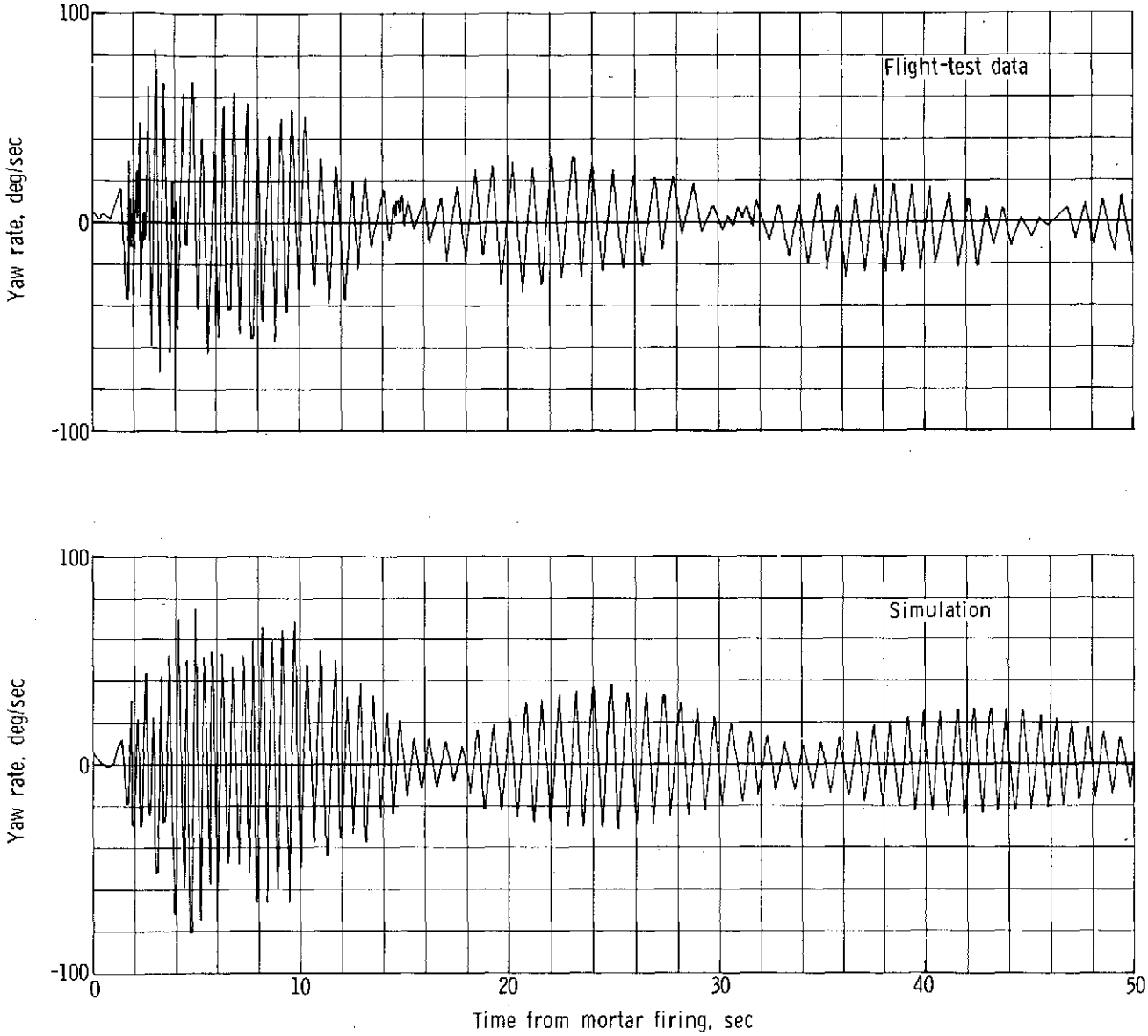

Figure 16.- Vehicle yaw-rate comparison.

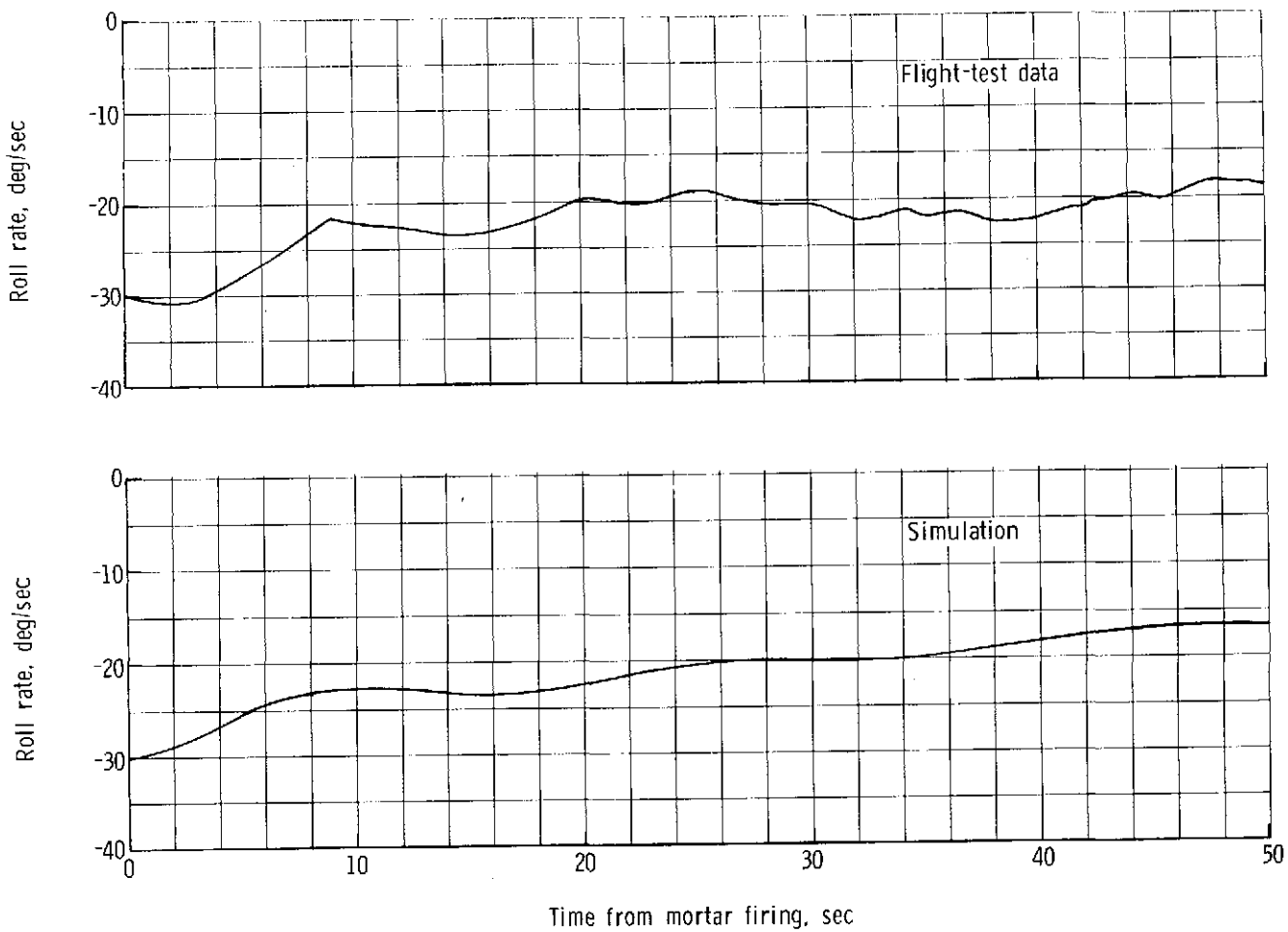

Figure 17.- Vehicle roll-rate comparison.

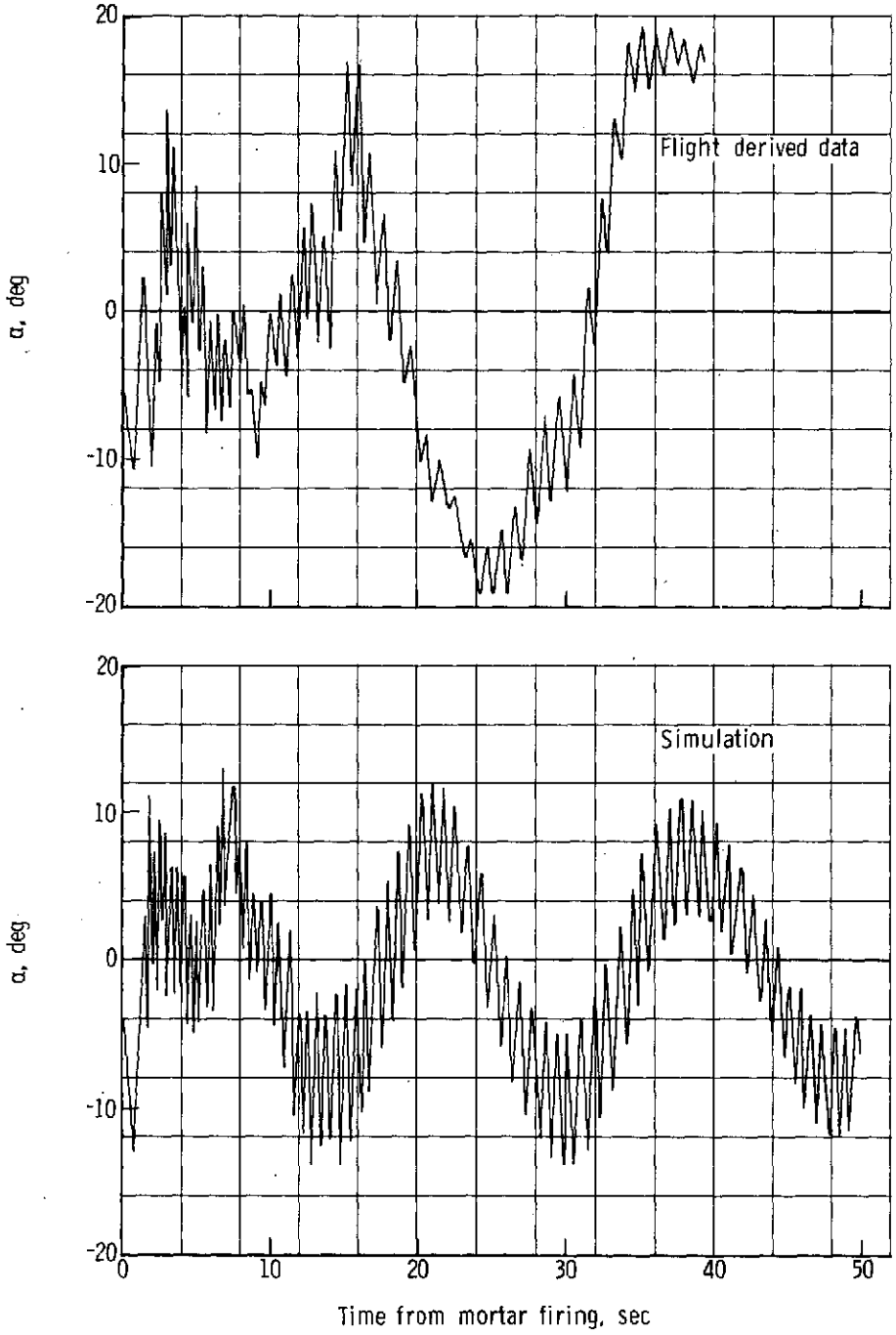

Figure 18.- Vehicle angle-of-attack comparison.

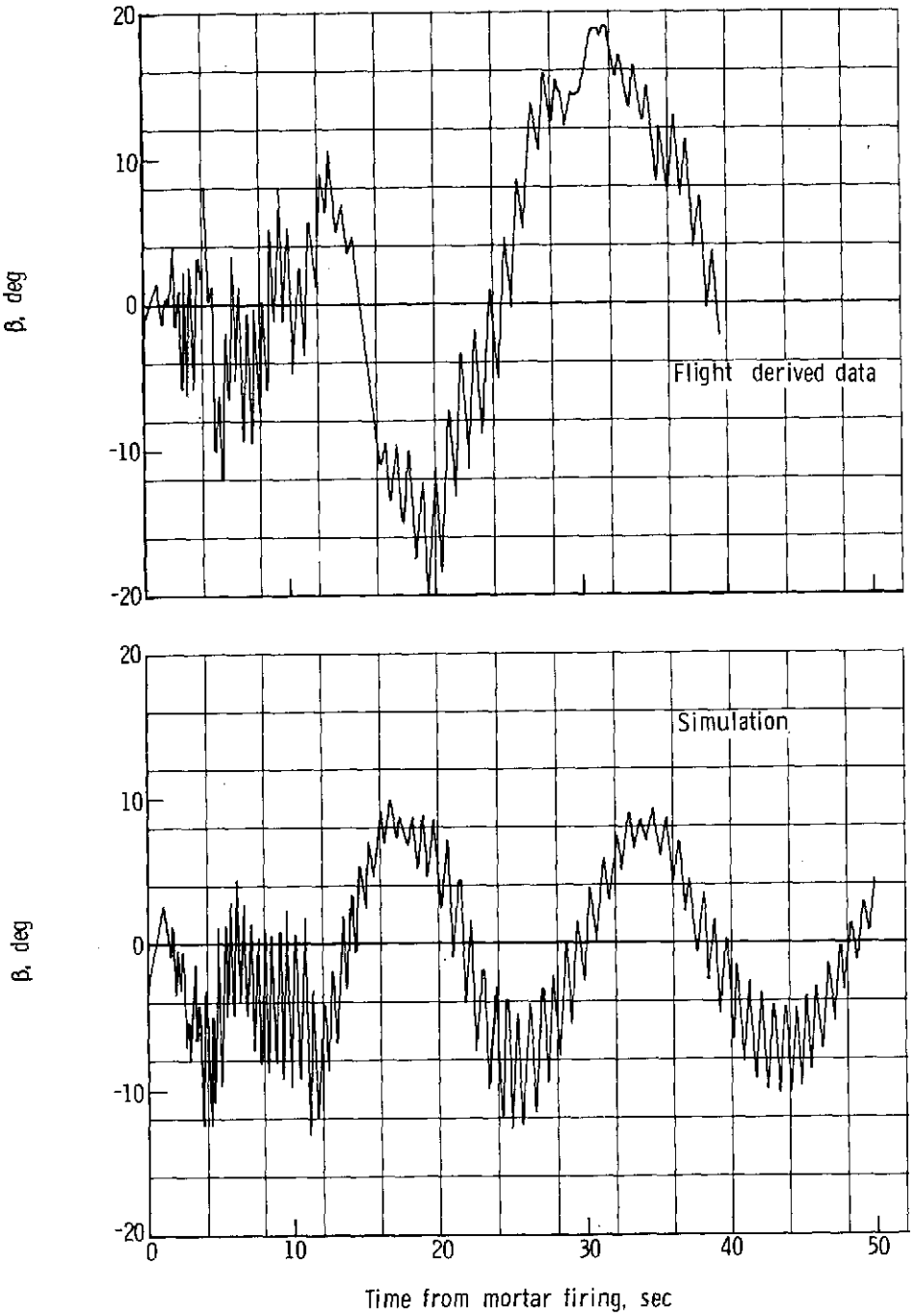

Figure 19.- Vehicle angle-of-sideslip comparison.

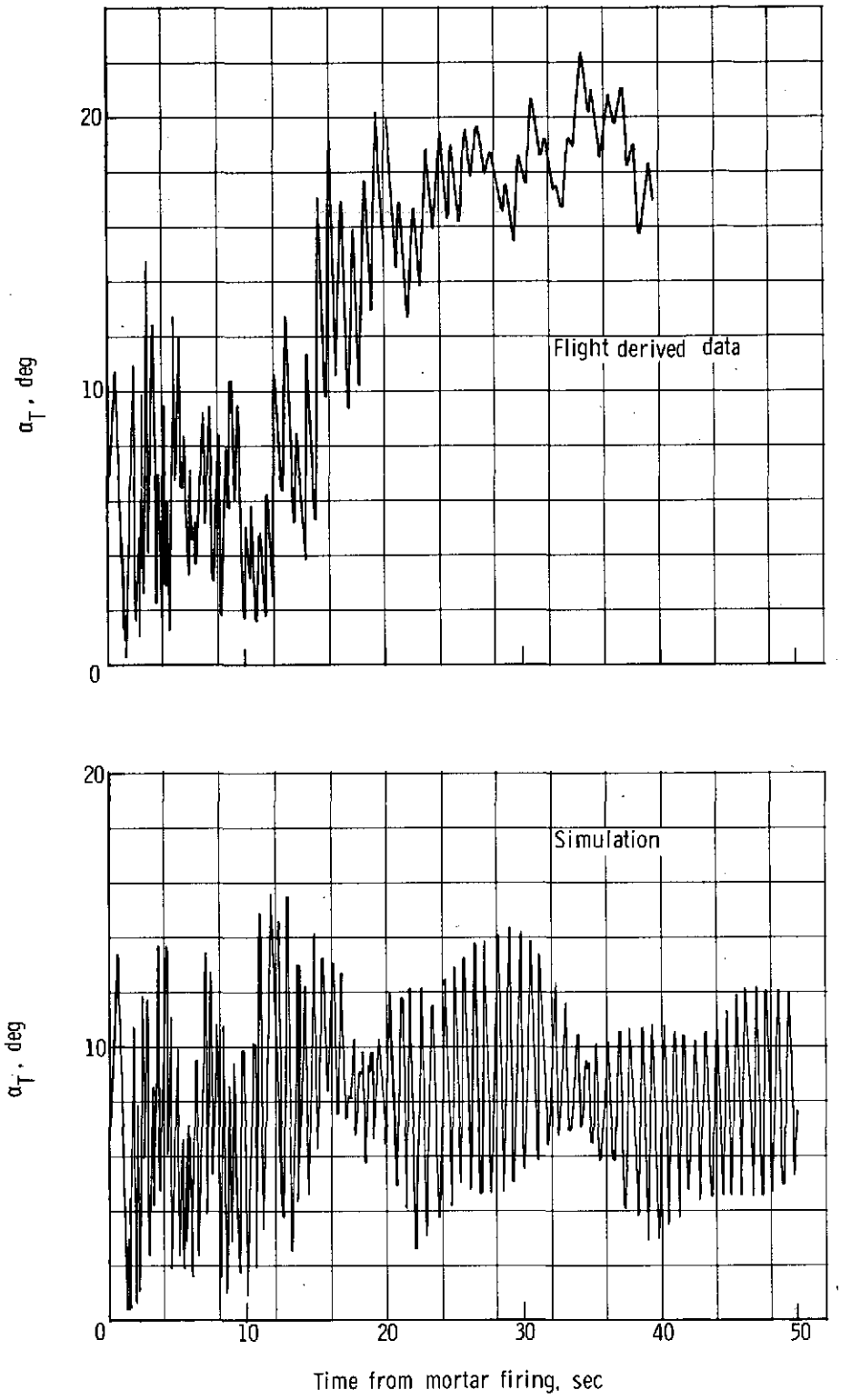

Figure 20.- Vehicle total angle-of-attack comparison.